JOURNAL OF PETROLOGY | VOLUME 45 | NUMBER 2 | PAGES 253–273 | 2004 | DOI: 10.1093/petrology/egg110

Thermal History of the Horoman Peridotite Complex: A Record of Thermal Perturbation in the Lithospheric Mantle

KAZUHITO OZAWA*

DEPARTMENT OF EARTH AND PLANETARY SCIENCE, GRADUATE SCHOOL OF SCIENCE, UNIVERSITY OF TOKYO, TOKYO 113-0033, JAPAN

RECEIVED NOVEMBER 27, 2002; ACCEPTED SEPTEMBER 19, 2003

The ascent history of the Horoman peridotite complex, Hokkaido, northern Japan, is revised on the basis of a detailed study of large ortho- and clinopyroxene grains ~1 cm in size (megacrysts) in the Upper Zone of the complex. The orthopyroxene megacrysts exhibit distinctive M-shaped Al zoning patterns, which were not observed in porphyroclastic grains less than 5 mm in size described in previous studies. Moreover, the Al and Ca contents of the cores of the orthopyroxene megacrysts are lower than those of the porphyroclasts. The Upper Zone is inferred to have resided not only at a higher temperature than previously suggested but also at a higher pressure (~1070°C, ~2·3 GPa) than the Lower Zone (~950°C, ~1·9 GPa), in the garnet stability field, before the ascent of the two zones. The Horoman complex probably represents a 12 ± 5 km thick section of lithospheric mantle with an ~10 ± 8°C/km vertical thermal gradient. The current thickness of the Horoman complex is ~3 km, which is a result of shortening of the lithospheric mantle by ~0·25 ± 0·1 during its ascent. The Upper Zone appears to have experienced a heating event during its ascent through the spinel stability field, with a peak temperature as high as 1200°C. The effect of heating decreases continuously towards the base of the complex, and the lowermost part of the Lower Zone underwent very minor heating at a pressure higher than ~0·5 GPa. The uplift and associated deformation, as well as heating, was probably driven by the ascent of a hot asthenospheric upper-mantle diapir into the Horoman lithosphere.

KEY WORDS: *Horoman;* P–T *trajectory; thermal history; Al diffusion in pyroxene; geothermobarometry*

INTRODUCTION

Records of the pressure–temperature history preserved in mantle peridotites provide important information to constrain the ascent rate of mantle materials and the mechanism of their emplacement into the lower crust. Particularly valuable is the spatial variation of P–T history preserved in a single peridotite body (e.g. MacGregor & Basu, 1976; Obata, 1980; Ozawa & Takahashi, 1995), which provides information on the dynamics of heat and material transfer from the mantle to the crust when combined with geological mapping of the complex (Nicolas, 1989; Sawaguchi & Takagi, 1997).

Three types of P–T history (or trajectory) of mantle materials initially located at depths as deep as the garnet stability field have been recognized for mantle peridotites on the basis of petrological and mineralogical studies. The first type features nearly adiabatic ascent at high temperature and pressure, followed by a rapid drop in temperature at a certain depth (Obata, 1980; Tubía, 1994; Ozawa & Takahashi, 1995; Van Roermund *et al.*, 2000; Drury *et al.*, 2001; Paquin & Altherr, 2001*a*). The second type is characterized by a non-adiabatic ascent path [greater dT/dP than the first type (Kornprobst, 1969; Obata, 1980; Davies *et al.*, 1993; Yang *et al.*, 1993; Kadarusman & Parkinson, 2000; Tsai *et al.*, 2000)], which suggests effective heat loss from the beginning of the ascent history. The third type involves a temperature rise by heating at a shallower depth, subsequent to either an adiabatic or a non-adiabatic ascent path (Van der Wal & Vissers, 1993; Ozawa, 1997; Nimis & Trommsdorff, 2001). More complex P–T trajectories, which can be combinations of the above three types, have also been proposed (Loubet & Allègre, 1979; Van der Wal & Vissers, 1993; Brenker & Brey, 1997). Such differences in the ascent history should reflect differences in the mode of thermo-mechanical interaction of the uplifting mantle with the adjacent lithospheric or asthenospheric

*Corresponding author. Telephone: +81-3-5841-4509. Fax: +81-3-5841-4569. E-mail: Ozawa@eps.s.u-tokyo.ac.jp

Table 1: Geological, petrographical, and mineralogical contrasts between the Upper and Lower Zones of the Horoman peridotite complex

Upper Zone	Lower Zone
Geological contrasts	
• Frequent occurrence of mafic layers alternating with peridotites	• Less frequent occurrence of mafic layers
• Thin frequent alternation of mafic and ultramafic rocks	• Thick layers of peridotite
• Sharp layer boundaries	• Gradational layer boundaries
• Plagioclase lherzolite predominant	• Harzburgite–spinel lherzolite predominant
• Very rare occurrence of symplectite-bearing spinel lherzolite	• Common occurrence of symplectite-bearing spinel lherzolite
• Association of banded dunite–harzburgite suite	• No known occurrence of banded dunite–harzburgite suite
• Common occurrence of plagioclase (segregation) veins	• Rare occurrence of plagioclase (segregation) veins
Petrographical contrasts	
• Common isolated plagioclase grains	• Rare isolated plagioclase grains
• Coarser and equigranular 'fine-grained aggregate' after two-pyroxene spinel symplectites	• Finer and elongated 'fine-grained aggregate' after two-pyroxene spinel symplectites
• Abundant exsolution lamellae of cpx in opx	• Minor exsolution lamellae of cpx in opx
• Rare occurrence of two-pyroxene spinel symplectites	• Common occurrence of two-pyroxene spinel symplectites
• Large grain size of two-pyroxene spinel symplectites	• Small grain size of two-pyroxene spinel symplectites
• Common equigranular (polygonal) textures	• Mostly porphyroclastic texture with basal mylonitic zones
• Equigranular small olivine grains with minor subgrain boundaries	• Elongated large olivine grain with many subgrain boundaries
• Small average grain size of orthopyroxene porphyroclasts	• Large average grain size of orthopyroxene porphyroclasts
• Top-to-the-south sense of shear dominant	• Top-to-the-north sense of shear dominant
Mineralogical contrasts	
• An-rich plagioclase in plagioclase lherzolites	• An-poor plagioclase in plagioclase lherzolites
• Less heterogeneous An distribution in each plagioclase grain	• Strongly zoned plagioclase grains in An content
• High Cr/(Cr + Al) ratio of chromian spinel	• Low Cr/(Cr + Al) ratio of chromian spinel
• More homogeneous spinel Cr/(Cr + Al) in each sample	• Markedly heterogeneous spinel Cr/(Cr + Al) in each sample
• Rare M-shaped Al zoning in pyroxene porphyroclasts	• Common M-shaped Al zoning in pyroxene porphyroclasts
• High Al content in pyroxene cores less than ~5 mm in size	• Low Al content in pyroxene cores less than ~5 mm in size
• High Ca content in orthopyroxene porphyroclast cores	• Low Ca content in orthopyroxene porphyroclast cores
• Low Ca content in clinopyroxene porphyroclast cores	• High Ca content in clinopyroxene porphyroclast cores

Data sources: Komatsu & Nochi (1966), Niida (1975, 1984), Takahashi & Arai (1989), Takahashi (1991, 1997, 2001), Ozawa & Takahashi (1995), Sawaguchi & Takagi (1997), Takazawa *et al*. (1999). The mineralogical contrasts are mostly for plagioclase lherzolites.

mantle and lower crust. They could also indicate the thermal effects of a melt segregated from the asthenosphere or much deeper mantle.

The Horoman peridotite complex is ideal for study of such thermo-mechanical interactions. The complex is distinguished by its exceptional freshness, with very minor degrees of low-temperature alteration, and the presence of symplectic aggregates inferred to be a breakdown product of garnet (Kushiro & Yoder, 1966; Tazaki *et al.*, 1972). These two features are closely related to its ascent history, particularly to the ascent rate or the cooling rate.

Early workers noted that the Horoman peridotite complex consists of upper and lower units with contrasting features in terms of lithology, structure and olivine fabric; these are called the Upper Zone and Lower Zone, respectively (Komatsu & Nochi, 1966; Niida, 1975, 1984; Table 1). Ozawa & Takahashi (1995) studied the thermal history of the Horoman complex for the first time. They examined the chemical zoning of orthopyroxene porphyroclasts (up to 5 mm) in plagioclase lherzolites and discovered M-shaped Al zoning patterns in the Lower Zone, but they found only bell-shaped Al zoning patterns in the Upper Zone. The Al contents of the cores of the bell-shaped orthopyroxenes from the Upper Zone are higher than the Al contents in the cores of M-shaped orthopyroxenes in the Lower Zone. Ozawa & Takahashi

(1995) also noted that the Ca contents of the orthopyroxene cores gradually increase from the base to the top of the complex. These mineral chemical data clearly demonstrate that the Upper Zone followed a higher-temperature decompression path than the Lower Zone.

Ozawa & Takahashi (1995) argued that the decompression path was nearly adiabatic up to the plagioclase–spinel facies boundary followed by a rapid cooling along the boundary and that the differences in the temperature of the ascent paths were principally due to differences in the initial temperatures within the garnet stability field. The initial depth of equilibration for the two zones was constrained at ~2 GPa, but this was only a minimum estimate. The most important observation of the absence of M-shaped Al zoning patterns in orthopyroxene porphyroclasts with grain size up to 5 mm from the Upper Zone was simply explained by its initial higher temperature condition and subsequent adiabatic ascent path, which allowed the marginal Al peak in the zonation pattern to flatten out. In contrast, the M-shaped Al zoning patterns preserved in the Lower Zone were explained by a lower initial temperature and low-T adiabatic exhumation path.

Takazawa *et al.* (1996) estimated P–T conditions for the 'primary' and 'secondary' stages for peridotites from the upper horizon of the Lower Zone by applying several geothermobarometers to pyroxene cores and neoblasts. They estimated a 'primary' temperature ~100°C higher than that of Ozawa & Takahashi (1995), even if the location of the horizon studied by Takazawa *et al.* (1996) is taken into consideration. The discrepancy must be reconciled to better constrain the absolute P–T conditions of equilibration in the mantle before the ascent of the Horoman complex.

In a subsequent paper, Ozawa (1997) modeled the development of M-shaped Al zoning patterns in the Lower Zone orthopyroxene porphyroclasts and demonstrated that the difference in orthopyroxene zoning patterns between the Upper and Lower Zones could be produced by two different model exhumation paths. The first involves an adiabatic decompression path for the Lower Zone with a significantly different initial temperature from the Upper Zone, in the garnet stability field. The second involves similar starting conditions in the garnet field, subsequently followed by adiabatic decompression with a temperature rise within the spinel field only for the Upper Zone. The second model provides an alternative way to explain not only the presence of M-shaped Al zoning patterns in orthopyroxene from the Lower Zone but also the common occurrence of a marginal hump in the Ca content of the orthopyroxene porphyroclasts in the Upper Zone, which is too high to be induced by an adiabatic path.

Interpretation of M-shaped Al zoning patterns in orthopyroxene from the Alpe Arami garnet peridotite body (Paquin & Altherr, 2001*a*) has recently provoked a controversy. Paquin & Altherr (2001*b*) argued for a nearly isothermal decompression path from the peak metamorphic conditions of 1180°C and 5·9 GPa followed by a rapid cooling at ~1 GPa, whereas Nimis & Trommsdorff (2001) argued against this model and proposed a two-stage P–T history whereby the Alpe Arami body was equilibrated at ~800°C and 3 GPa and was subsequently subjected to a short-lived thermal event at a temperature higher than 1100°C.

It is, therefore, still debatable if the apparent difference in the thermal history of the Upper and Lower Zones of the Horoman complex is due to a difference in the initial temperature within the garnet stability field or if the Upper Zone went through a subsequent heating event within the spinel stability field. The argument comes from ambiguity in the significance of the core composition of the orthopyroxene porphyroclasts, particularly those from the higher-temperature Upper Zone. The size of the largest porphyroclasts examined in previous studies (e.g. Ozawa & Takahashi, 1995) was less than ~5 mm. Such porphyroclasts from the Upper Zone do not show the characteristic M-shaped Al profile and do not have a wide core region with uniform Al and Ca distribution. The size of 5 mm may not be large enough to have recorded any meaningful P–T conditions in the garnet stability field in the Upper Zone.

The purpose of this paper is further to constrain the ascent history of the Horoman peridotite complex by examining centimeter-sized orthopyroxene and clinopyroxene crystals (megacrysts) in plagioclase lherzolites of the Upper Zone. The new results suggest that the P–T history proposed by Ozawa & Takahashi (1995) should be revised. Moreover, this revised P–T trajectory allows discussion of the initial conditions in the Horoman peridotite complex mantle and the processes that controlled its ascent into the lower crust.

GEOLOGICAL BACKGROUND AND STUDIED SAMPLES

The Horoman peridotite complex, Hokkaido, Japan is located at the southern end of the Hidaka metamorphic belt (Fig. 1), which is characterized by a low-P/high-T type of metamorphism in Paleogene to early Miocene times. The Hidaka belt represents an ~23 km thick sequence including the upper-mantle and crustal section of a magmatic arc (Komatsu *et al.*, 1983). The Horoman complex occupies the tectonically lowest horizon of the Hidaka belt and is approximately 8 km × 10 km in size.

The Horoman complex is stratified and its total thickness is estimated to be ~3 km (Niida, 1984). Niida (1984) divided the complex into Upper and Lower Zones based on the contrasting geological characteristics of the two

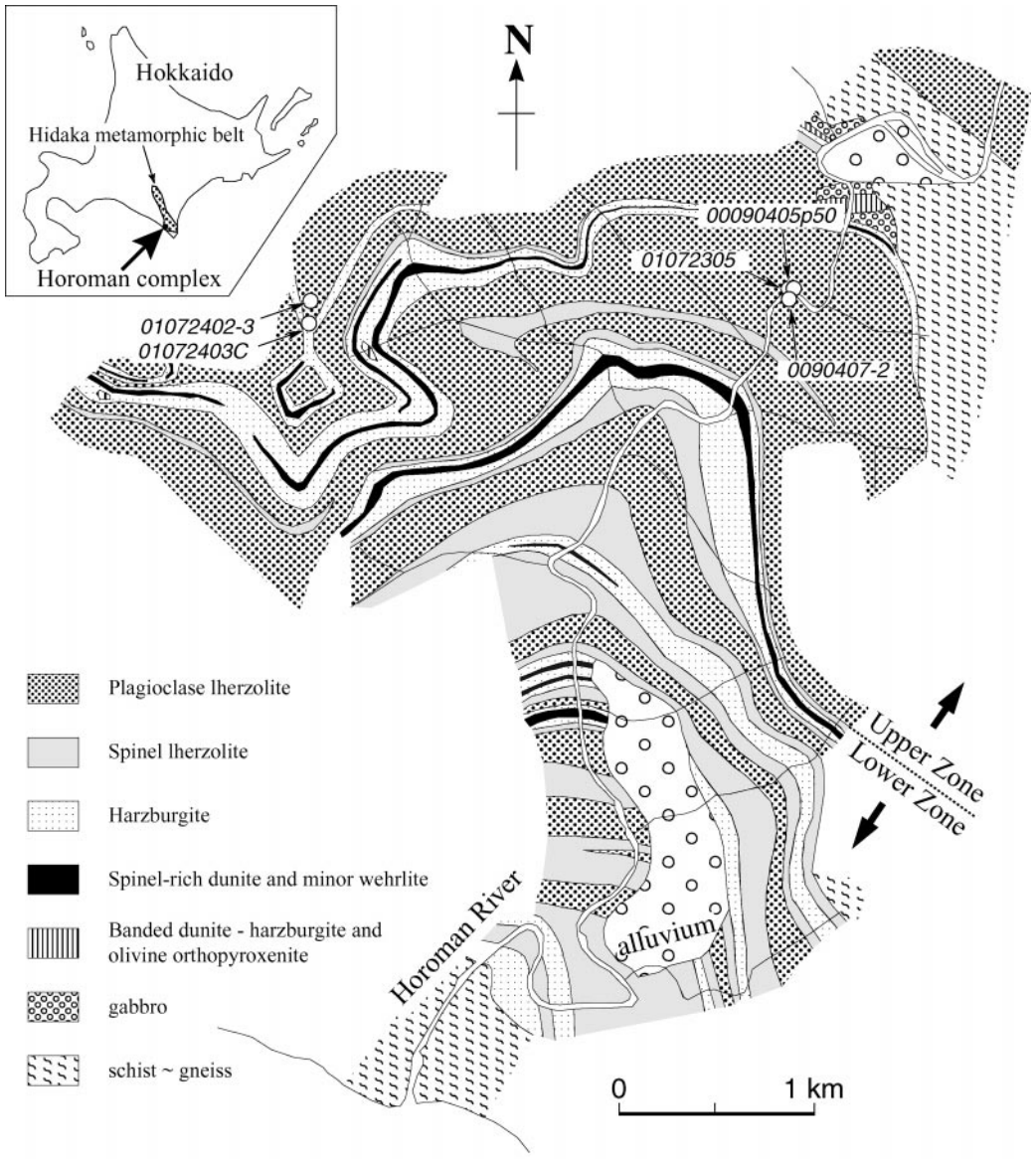

Fig. 1. Geological map of the Horoman complex after Takahashi (1992), showing the sample localities of the plagioclase lherzolites containing large orthopyroxene or clinopyroxene megacrysts. All the samples are from the Upper Zone. In addition to the gabbros shown in the map, mafic layers with thickness 1 cm–5 m are interlayered with the peridotites dominantly within the Upper Zone (Takazawa *et al.*, 1999).

zones (Table 1). The Lower Zone is composed mainly of alternating layers of plagioclase lherzolite, spinel lherzolite (with or without two-pyroxene symplectites after garnet), and harzburgite with lesser amount of spinel-rich dunite–wehrlite layers. It shows cyclic layering whose half cycle starts from plagioclase lherzolite and ends in spinel-rich dunite, through symplectite-bearing spinel lherzolite, symplectite-free spinel lherzolite, and harzburgite (Fig. 1; Komatsu & Nochi, 1966; Niida, 1984; Obata & Nagahara, 1987; Takahashi, 1992). The lithological boundaries are gradational except for the sharp contact between dunite and harzburgite. The thickness of each cycle ranges from 200 to 600 m. Minor amounts of mafic layers (~1·2% in volume; Takazawa *et al.*, 1999) are also present.

The Upper Zone is composed of rock types similar to the Lower Zone, but plagioclase lherzolite is more abundant (Fig. 1). Mafic layers are more dominant in this zone (~2·1 vol. %) as compared with the Lower Zone (Table 1; Takazawa *et al.*, 1999). Plagioclase-rich segregation veins locally cut the plagioclase lherzolites, oriented parallel to the lineation but oblique to the foliation. The veins are composed mostly of Na-rich plagioclase with minor amount of Ti-rich pargasite and/or phlogopite and are absent in the lower ~120 m above the boundary with the Lower Zone (Takahashi, 1997). This type of vein is

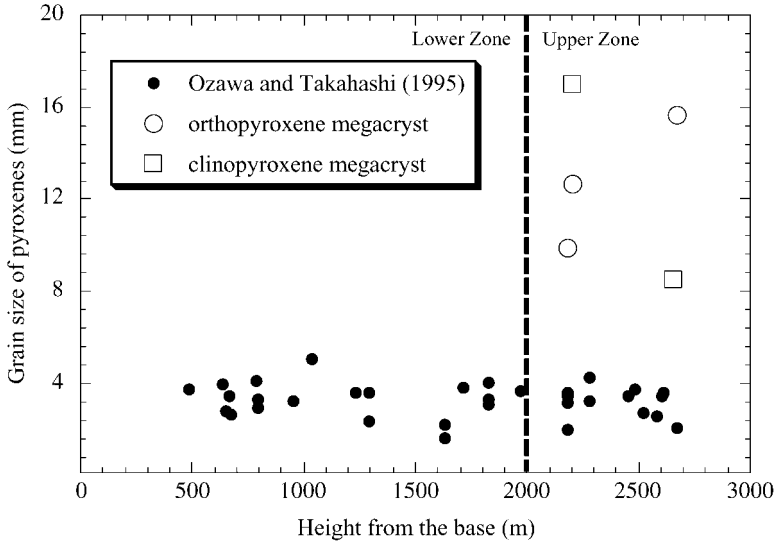

Fig. 2. Grain size of orthopyroxene crystals in plagioclase lherzolite plotted against the height from the base of the complex, calculated according to the geological map of Niida (1974). The size measurement was made from thin sections. The sizes of the orthopyroxene megacrysts examined in this study are shown with open symbols, and those of large porphyroclasts studied by Ozawa & Takahashi (1995) with filled symbols. The grain size of orthopyroxene, except for the megacrysts, tends to decrease slightly with the height from the base, which is attributable to deformation under the higher-temperature conditions in the Upper Zone.

frequently observed in the Nikanbetsu complex, located about 9 km to the east of the Horoman complex, which has lithological and petrographic features similar to the Upper Zone of the Horoman complex (Niida & Katoh, 1978).

Plagioclase lherzolite samples containing large pyroxene crystals (megacrysts) were collected from two horizons in the Upper Zone (Fig. 1). One locality is along the Horoman River, ~200 m above the boundary with the Lower Zone. The other is on the North Ridge of Mt. Apoi, ~700 m above the zone boundary. Two orthopyroxene and one clinopyroxene megacrysts were sampled from the Horoman River locality, and one orthopyroxene and one clinopyroxene from the North Ridge locality. The pyroxene megacrysts, which usually occur in a plagioclase-rich layer, are ~1–2 cm in size (Fig. 2) with their long axes lying nearly parallel to the layering. They occur sporadically and never form clusters. The plagioclase-rich layer is often thinner than the pyroxene grains, showing a boudinage-like structure, and the megacrysts tend to have wide contact with the peridotite host.

Figure 2 shows the size of the studied pyroxene megacrysts in comparison with the size of the largest orthopyroxene porphyroclasts in both Lower and Upper Zone plagioclase lherzolite reported by Ozawa & Takahashi (1995). The size of the porphyroclasts in the normal plagioclase lherzolites is always less than 5 mm, and tends to decrease slightly with height above the base. In contrast, the megacrysts associated with the plagioclase-rich layers in the Upper Zone reach 8–17 mm in size and are 2–3 times larger than the largest porphyroclasts.

ANALYTICAL METHODS

Electron probe microanalyses were conducted with JEOL electron microprobe analyzers JXA-8900L and JCMA733-MkII at the Department of Earth and Planetary Science, Graduate School of Science, University of Tokyo. Analytical conditions for point and line analyses are 15 kV accelerating voltage and $1{\cdot}2 \times 10^{-8}$ A current measured with the Faraday cup. A focused beam was used except for line analyses of pyroxenes, for which a 20 μm diameter beam was used to obtain the bulk composition including exsolution lamellae. Counting time was 30 s for each element, but 10 s was used in the line analyses of pyroxenes to maximize the total number of analyzed points, from which averaged compositions were obtained for the core or marginal part. The ZAF correction scheme was used to reduce counts to oxide concentrations. In map analyses, conditions of $2{\cdot}0 \times 10^{-7}$ A current, 5 μm beam size, 5–20 μm pixel size, and 30–50 ms count time at each point were used.

MINERAL CHEMISTRY OF THE HOROMAN COMPLEX: NEW RESULTS

Chemical zoning of large pyroxene porphyroclasts from the Upper Zone

Figure 3 shows the Al and Ca distribution in a large orthopyroxene megacryst in a plagioclase lherzolite from the North Ridge locality (Table 2). Marginal

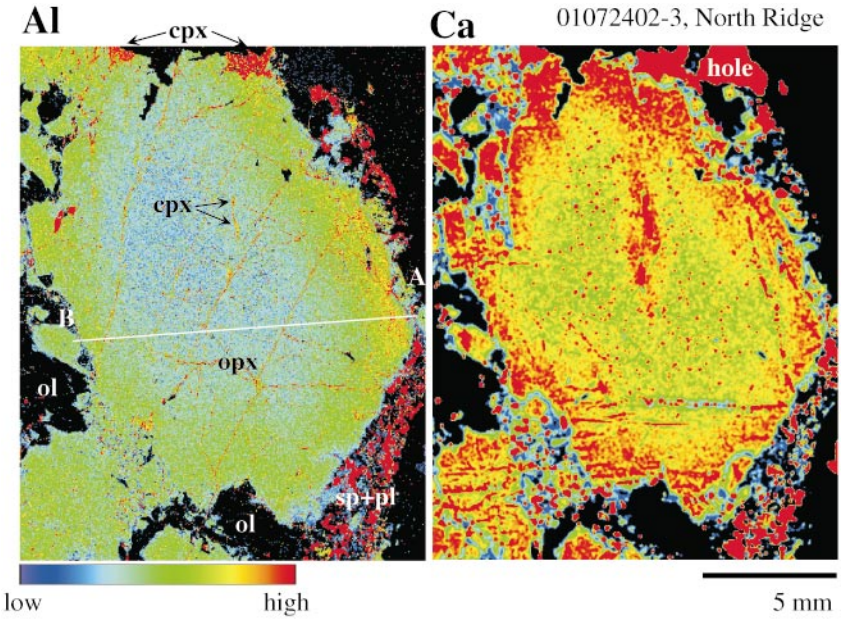

Fig. 3. X-ray maps showing Al and Ca distributions in a large orthopyroxene megacryst in a plagioclase lherzolite from the Upper Zone (01072402-3, North Ridge) of the Horoman complex. There is a seam composed of fine-grained spinel and plagioclase in contact with the megacryst on the right-hand side. To enhance the contrast in the Ca map, the image was processed with a smoothing filter. It should be noted that Al and Ca are high in the marginal zone of the orthopyroxene megacryst. There are elongate clinopyroxene grains near the center, which disturb the concentric Ca zoning pattern. A–B indicates the line profile shown in Fig. 4. The marginal Al content is higher on the right-hand side, as a result of the presence of the fine-grained seam.

enrichment in Al and Ca is evident. The zoning patterns are concentric, although elongate clinopyroxene blebs near the center somewhat disturb the concentric zoning pattern of Ca. In line profiles, the Al and Ca contents have a marginal peak, from which the contents sharply decrease towards the rim and gradually decrease towards the relatively homogeneous core (Fig. 4). The variation in Al is counterbalanced by Si and Mg + Fe as shown in Fig. 4, and thus attributable to the Tschermak substitution, Si(Mg,Fe) ⇔ AlAl. A smaller grain (5 mm in size), present in the lower left corner in the Al and Ca maps (Fig. 3), displays zoning which monotonously decreases in Al and Ca from the center to the rim. Other orthopyroxene megacrysts from the Horoman River locality have similar Al and Ca zoning patterns.

Figure 5 shows the Al and Na distribution in a large clinopyroxene megacryst in a plagioclase lherzolite from the Horoman River locality (Table 2). As in the case of the orthopyroxene megacryst, Al shows concentric zoning with a marginal maximum, from which the Al content sharply decreases towards the rim and gradually decreases toward the core (Figs 5 and 6). This clinopyroxene has large blebs of orthopyroxene (~1 mm across) and plagioclase in the center, where the Al content of the host tends to be broadly constant but with some scatter (Fig. 6). The presence of such blebs makes it difficult to determine the bulk compositional variation in the clinopyroxene.

The plagioclase blebs are low in An [100 × Ca/(Ca + Na) ~46] compared with the plagioclase surrounding the clinopyroxene (An >60). A few domains consisting of several apparently isolated plagioclases with the same optical orientation were identified. The orthopyroxene blebs are optically continuous, suggesting that they were exsolved from the host clinopyroxene. The domain structure of the plagioclase blebs, intimately associated with the orthopyroxene blebs, suggests exsolution of plagioclase from a super-silicic clinopyroxene enriched in the Ca-Eskola component (Gasparik, 1985). The size of the blebs suggests that the exsolution started at an earlier stage of, or even before, the decompression to give enough time to grow to 1 mm in size. Clinopyroxene containing large plagioclase and orthopyroxene blebs is common as porphyroclasts in the Upper Zone, and fine-grained 'inclusions' of albite and quartz of <20 μm in size have also been reported in clinopyroxene porphyroclasts from the Lower Zone (Takahashi, 1997). These albite and quartz inclusions could also have been exsolved from a super-silicic clinopyroxene (Kitayama *et al.*, 2000).

In addition to blebby orthopyroxene in the core, there are smaller and aligned elongate orthopyroxene grains in the marginal zone (Fig. 5). The morphology and uniform optical orientation, sharing the *c*-axis with the host clinopyroxene, clearly suggests that the orthopyroxene in this zone was exsolved from the host. The profile of Ca/(1 − Na), which is a good indicator of temperature for

Table 2: Average compositions of cores, marginal zones and representative rim compositions of orthopyroxene and clinopyroxene megacrysts in plagioclase lherzolites from the Upper Zone of the Horoman complex

	Orthopyroxene															Clinopyroxene									
	00090407-2					00090405+50					01072402-3					1072305					01072403C				
	core		margin		rim	core		margin		rim	core		margin		rim	core		margin		rim	core		margin		rim
	av.	1σ	av.	1σ	def.	av.	1σ	av.	1σ	foc.	av.	1σ	av.	1σ	def.	av.	1σ	av.	1σ	foc.	av.	1σ	av.	1σ	foc.
wt %																									
SiO_2	55·90	0·23	55·15	0·13	55·90	56·28	0·48	55·83	0·21	56·12	55·87	0·26	54·55	0·25	55·67	53·17	0·95	51·00	1·08	52·32	53·54	1·66	50·95	0·64	51·17
Al_2O_3	3·02	0·13	4·08	0·12	2·42	2·92	0·44	4·35	0·04	2·01	2·94	0·16	4·52	0·12	2·32	3·26	0·58	5·51	0·28	3·89	2·67	0·52	5·27	0·40	4·02
TiO_2	0·13	0·03	0·15	0·02	0·22	0·19	0·06	0·20	0·03	0·15	0·19	0·03	0·16	0·02	0·18	0·30	0·07	0·37	0·12	0·43	0·39	0·15	0·71	0·15	0·89
FeO	5·96	0·27	5·97	0·22	5·99	5·99	0·27	6·50	0·21	6·76	5·92	0·25	5·86	0·21	6·92	3·45	1·28	3·66	1·25	2·81	4·35	1·99	2·96	0·51	2·93
MnO	0·16	0·04	0·15	0·03	0·10	0·13	0·04	0·18	0·03	0·22	0·13	0·04	0·15	0·03	0·14	0·10	0·05	0·09	0·03	0·10	0·12	0·06	0·09	0·04	0·12
MgO	33·31	0·45	32·79	0·20	34·01	33·60	0·55	32·47	0·28	33·63	33·11	0·29	32·24	0·24	33·05	17·03	4·69	17·30	5·55	16·26	20·56	7·82	15·89	2·85	15·52
CaO	1·09	0·55	1·00	0·17	0·45	0·96	0·35	1·06	0·13	0·54	1·14	0·20	1·29	0·23	0·50	20·16	5·98	19·62	6·88	22·15	15·79	9·79	20·99	3·51	23·43
Na_2O	0·06	0·03	0·05	0·02	0·02	0·11	0·13	0·03	0·01	0·01	0·09	0·04	0·05	0·02	0·06	0·75	0·23	0·57	0·22	0·63	0·57	0·36	0·60	0·12	0·53
Cr_2O_3	0·43	0·06	0·55	0·08	0·56	0·40	0·07	0·44	0·02	0·34	0·45	0·07	0·57	0·07	0·42	1·28	0·20	1·22	0·14	0·96	1·44	0·50	1·37	0·10	1·15
NiO	0·10	0·04	0·09	0·04	0·06	0·11	0·04	n.a.	n.a.	0·00	0·12	0·04	0·14	0·03	0·07	0·05	0·02	n.a.	n.a.	n.a.	0·06	0·03	0·03	0·02	0·04
Total	100·17	0·48	99·99	0·37	99·73	100·70	0·48	101·06	0·36	99·87	99·94	0·53	99·53	0·38	99·33	99·56	0·56	99·34	0·45	99·55	99·49	0·77	98·86	0·71	99·79
Cation (O = 6)																									
Si	1·928	0·006	1·906	0·005	1·934	1·930	0·012	1·911	0·007	1·945	1·931	0·007	1·896	0·006	1·941	1·936	0·011	1·863	0·009	1·911	1·935	0·014	1·873	0·010	1·878
Al	0·123	0·005	0·166	0·005	0·099	0·118	0·018	0·175	0·002	0·082	0·120	0·006	0·185	0·005	0·095	0·140	0·026	0·237	0·016	0·168	0·114	0·024	0·228	0·019	0·174
Ti	0·003	0·001	0·004	0·001	0·006	0·005	0·002	0·005	0·001	0·004	0·005	0·001	0·004	0·001	0·005	0·008	0·002	0·010	0·003	0·012	0·011	0·004	0·020	0·004	0·024
Fe^{2+}	0·172	0·008	0·173	0·006	0·173	0·172	0·007	0·186	0·006	0·196	0·171	0·007	0·170	0·006	0·202	0·105	0·036	0·111	0·035	0·086	0·130	0·056	0·091	0·015	0·090
Mn	0·005	0·001	0·004	0·001	0·003	0·004	0·001	0·005	0·001	0·006	0·004	0·001	0·004	0·001	0·004	0·003	0·002	0·003	0·001	0·003	0·004	0·002	0·003	0·001	0·004
Mg	1·713	0·022	1·690	0·009	1·754	1·718	0·024	1·656	0·013	1·738	1·706	0·014	1·670	0·012	1·718	0·921	0·234	0·938	0·273	0·885	1·098	0·386	0·870	0·149	0·849
Ca	0·040	0·021	0·037	0·006	0·017	0·035	0·013	0·039	0·005	0·020	0·042	0·007	0·048	0·009	0·019	0·789	0·235	0·772	0·272	0·867	0·621	0·386	0·827	0·141	0·921
Na	0·004	0·002	0·003	0·001	0·001	0·008	0·009	0·002	0·001	0·001	0·006	0·002	0·004	0·002	0·004	0·053	0·017	0·041	0·016	0·044	0·041	0·026	0·043	0·009	0·037
Cr	0·012	0·002	0·015	0·002	0·015	0·011	0·002	0·012	0·001	0·009	0·012	0·002	0·016	0·002	0·011	0·037	0·006	0·035	0·004	0·028	0·041	0·015	0·040	0·003	0·033
Ni	0·003	0·001	0·002	0·001	0·002	0·003	0·001	n.a.	n.a.	0·000	0·003	0·001	0·004	0·001	0·002	0·001	0·001	n.a.	n.a.	n.a.	0·002	0·001	0·001	0·001	0·001
Total	4·003	0·006	4·001	0·003	4·004	4·004	0·007	3·991	0·007	4·004	4·001	0·006	4·002	0·005	4·002	3·995	0·009	4·011	0·006	4·003	3·997	0·008	3·995	0·005	4·012

av., average; def., defocused analysis (20 μm beam size); foc., focused analysis; n.a., not analyzed.

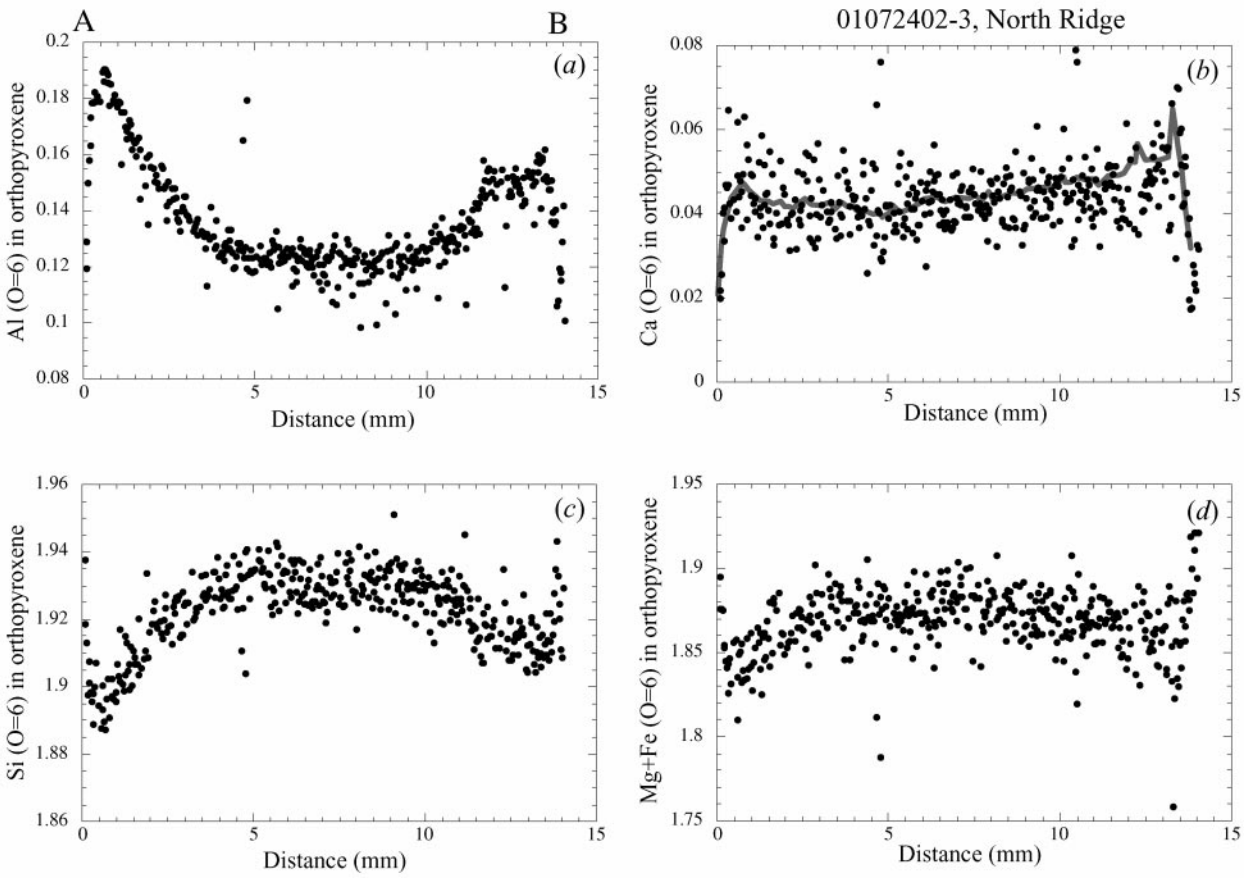

Fig. 4. EPMA line analysis across a large orthopyroxene grain from the Upper Zone (01072402-3, North Ridge) of the Horoman complex for Al, Ca, Si, and Mg + Fe cations (O = 6). The analyses were made with a defocused beam with a 20 μm beam size. The large scatter in Ca content is due to the exsolution of clinopyroxene. The variation of pyroxene composition including exsolution lamellae was obtained by taking a running average and is shown in (b) as a smooth grey curve, which suggests a marginal peak in Ca content. The location of this line profile is shown in Fig. 3.

pyroxene (Brey & Köhler, 1990), is shown in Fig. 6b together with a smoothed curve obtained by taking a running average including the orthopyroxene exsolution. The margin of the megacryst with abundant exsolution of orthopyroxene (Fig. 5) is low in Ca/(1 − Na). Such zoning, characterized by a marginal minimum, is also observed in smaller clinopyroxene porphyroclasts (<5 mm in size) in plagioclase lherzolite from the Lower Zone.

The Na content of the clinopyroxene megacryst decreases towards the rim in the marginal zone. There is an abrupt change in the Na content at the boundary between the marginal zone and the blebby core, where the Na content is rather constant. The Cr content is high in the core, and gradually decreases towards the rim, where it shows an abrupt decrease to ∼0·1. The overall zoning pattern is asymmetric and the decrease is more significant towards the rim in contact with plagioclase and spinel aggregates (Figs 5 and 6d). Another clinopyroxene from the North Ridge locality shows similar chemical zoning and internal microstructures to those described above (Table 2).

Spatial variation of core Al and Ca contents in orthopyroxene

The average compositions of the cores of the studied pyroxene megacrysts from the Upper Zone are summarized in Table 3. The Al and Wo contents [100 × Ca/(Ca + Mg + Fe)] in orthopyroxene are plotted against the height from the base of the Horoman complex in Fig. 7. In the Al diagram, the compositions of the smaller orthopyroxene crystals (porphyroclasts less than 5 mm in size) are also shown for comparison. It is noticeable that the Al contents of the cores of the large orthopyroxene megacrysts are significantly lower than those of grains smaller than 5 mm within the Upper Zone (Fig. 7a). The Al contents of the megacryst cores are similar to or slightly lower than those of the small orthopyroxene porphyroclasts from the Lower Zone.

On the other hand, the Wo content in the cores of the orthopyroxene megacrysts is similar to or lower than that of the smaller orthopyroxene porphyroclasts from the Upper Zone, but distinctly higher than that of porphyroclasts from the Lower Zone (Fig. 7b). If the high Wo

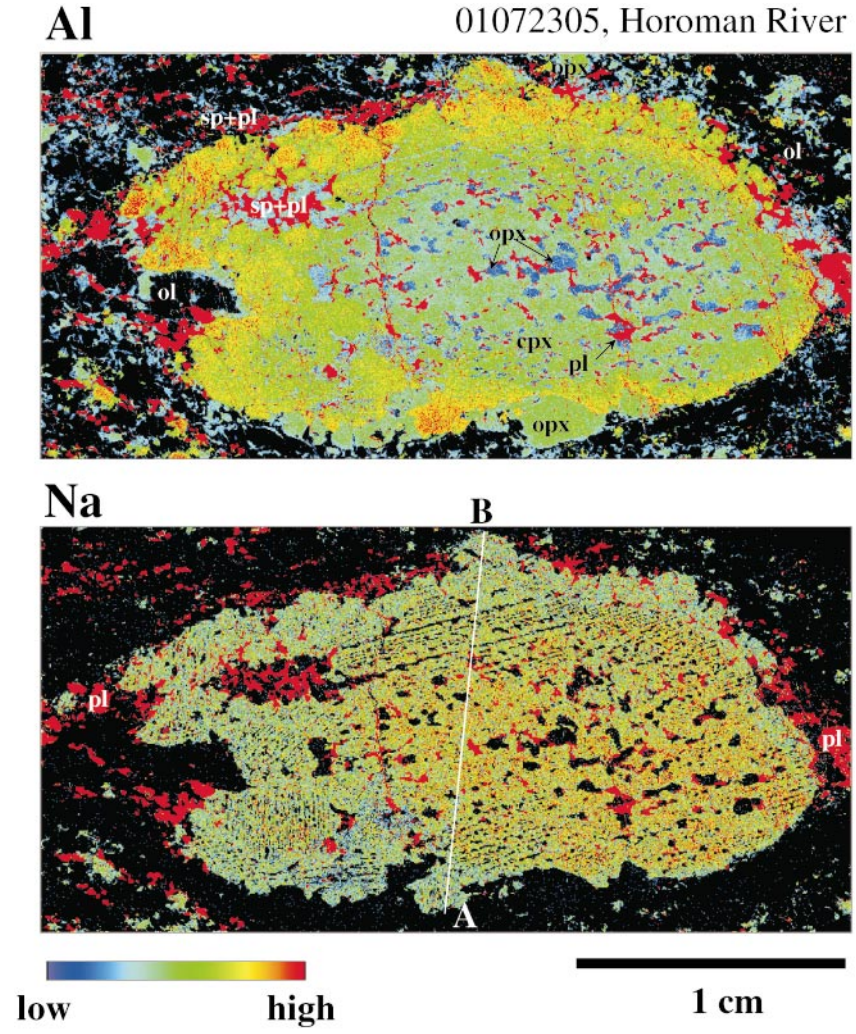

Fig. 5. X-ray maps showing Al and Na distributions in a large clinopyroxene megacryst in a plagioclase lherzolite from the Upper Zone (01072305, Horoman River) of the Horoman complex. The clinopyroxene megacryst contains large blebs of orthopyroxene and plagioclase. This plagioclase is more albitic than that occurring around the megacryst. It should be noted that the blebs are present only in the central region, where the Na content is higher and the Al content is lower than in the marginal zone. A–B indicates the line profile shown in Fig. 6.

values in the Upper Zone are ignored, there is a broadly linear increase in Wo content upwards in the complex from the middle of the Lower Zone, below which the Wo content is almost constant.

DISCUSSION

Petrographic constraints on the thermal history of the Horoman complex

In this section, petrographic observations that constrain the earliest and latest stages of the ascent history recorded in the Horoman peridotites are summarized. The former comes from the presence of two-pyroxene + spinel symplectites in symplectite-bearing spinel lherzolites, and the latter from plagioclase-rich, fine-grained aggregates in plagioclase lherzolites. Petrographic, mineralogical and geochemical information that unequivocally constrains the deep origin of the Horoman complex is the occurrence of the two-pyroxene + spinel symplectites frequently present in slightly depleted spinel lherzolite and rarely in plagioclase lherzolites. These aggregates are interpreted to be the breakdown product of garnet through reaction between olivine and garnet induced by the decompression of the Horoman complex (Takahashi & Arai, 1989; Takazawa *et al.*, 1996; Obata *et al.*, 1997; Yoshikawa & Nakamura, 2000).

The plagioclase lherzolites of the Horoman complex are unusual in the mode of occurrence of plagioclase. Plagioclase is completely restricted to fine-grained aggregates, composed mainly of plagioclase, olivine and chromite spinel, in the Lower Zone. These aggregates are

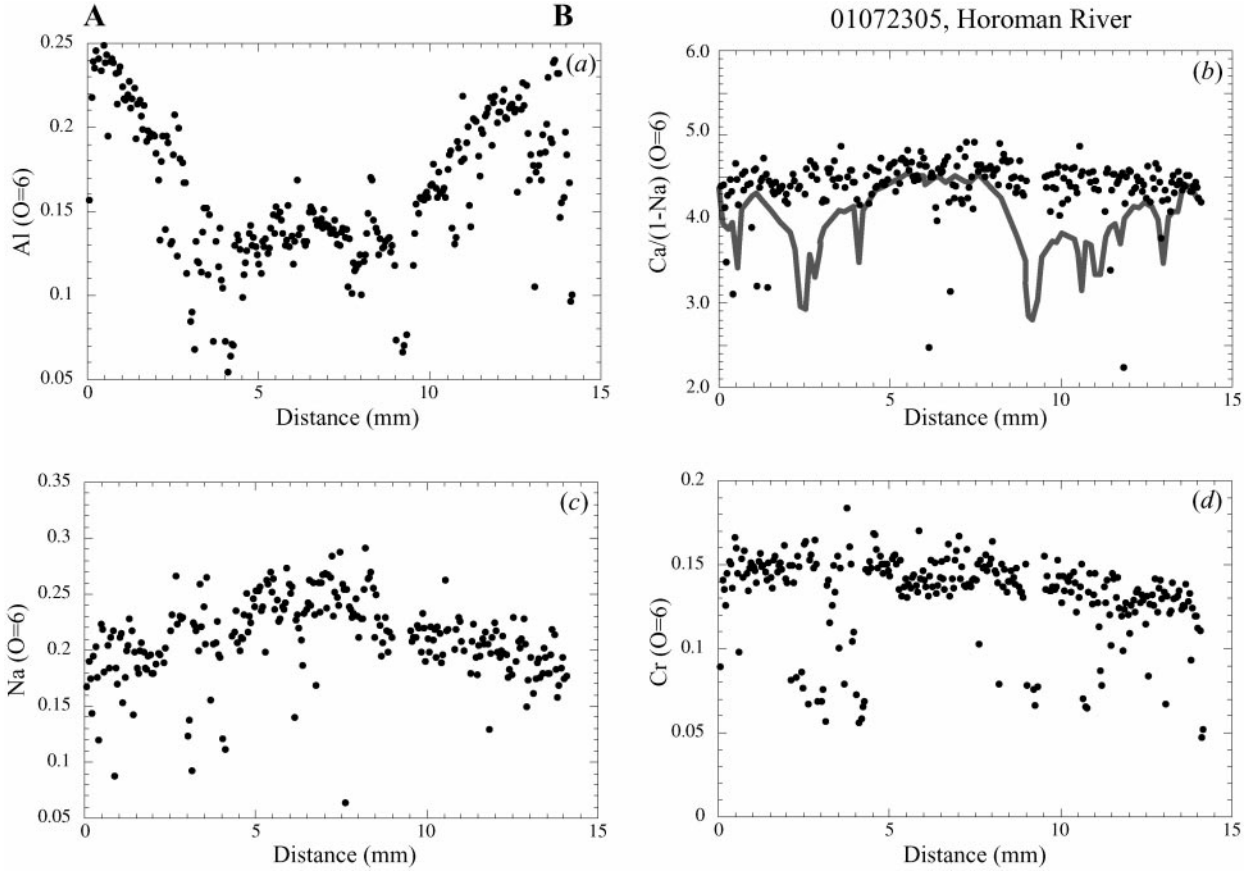

Fig. 6. EPMA line analysis across a large clinopyroxene megacryst from the Upper Zone (01072305, Horoman River) of the Horoman complex for Al, Ca/(1 − Na), Na, and Cr cations (O = 6). The analyses were made with a focused beam. The location of this line profile is shown in Fig. 5. Because the range of the Ca/(1 − Na) plot is > 2, the compositions of orthopyroxene inclusions plot far below the bottom abscissa. The occurrence of orthopyroxene grains can be easily recognized in the Al and Cr plots as lower concentration data points. The variation of pyroxene composition including exsolution lamellae was obtained by taking a running average of the raw profile and is shown in (b) as a smooth grey curve, which shows the presence of a marginal minimum.

Table 3: Averaged core compositions of large pyroxene grains from the Upper Zone of the Horoman complex

Mineral	Sample no.	Size (mm)	Wo	En	WoL	Ca (O = 6)	Al (O = 6)	Al(M1)	Al(M1)*	Others	Height (m)	Locality
Orthopyroxene	00090407-2	14 × 7	2·1 (11)	89·0 (11)	2·2 (11)	0·040 (21)	0·122 (5)	5·41 (33)	6·37 (27)	3·95 (73)	2180	Horoman River
	00090405 + 50	23 × 7	1·85 (70)	89·2 (7)	1·85 (71)	0·035 (13)	0·118 (18)	5·3 (12)	6·2 (11)	3·96 (94)	2200	Horoman River
	01072402-3	19 × 13	2·21 (39)	88·9 (5)	2·22 (39)	0·042 (7)	0·120 (6)	5·18 (38)	6·22 (31)	4·29 (80)	2670	North Ridge
Clinopyroxene	01072305	25 × 12	44 (13)	56 (11)	37 (12)	0·79 (23)	0·140 (26)	7·0 (17)	—	11·9 (24)	2200	Horoman River
	01072403C	9 × 8	34 (21)	58 (19)	29 (18)	0·62 (39)	0·114 (24)	4·6 (14)	—	9·5 (39)	2650	North Ridge

Numbers in parentheses indicate standard deviations (1σ) refering to the last decimal places. The crystal sizes are length and width measured in thin sections, the locations of which in pyroxene grains were carefully chosen to obtain the chemical composition in the grain center. Abbreviations: Wo = Ca/(Ca + Mg + Fe); En = Mg/(Ca + Mg + Fe); WoL, projected Wo value according to the method of Lindsley (1983); Al(M1), Al% in M1 site; Al(M1)*, Al% in M1 site extrapolated to Cr-free system according to Ozawa & Takahashi (1995); Others, total mol % of pyroxene components other than Wo, En and Fs.

interpreted to be a breakdown product of garnet through a two-pyroxene + spinel assemblage. The occurrence of plagioclase in the lherzolites is attributable to their bulk chemical composition, particularly the Na content. Decompression reactions continued to shallower levels and produced plagioclase (An 60–90) in Na-rich, fertile lherzolites, but did not in less fertile lherzolites (symplectite-bearing spinel lherzolites). This implies that the formation

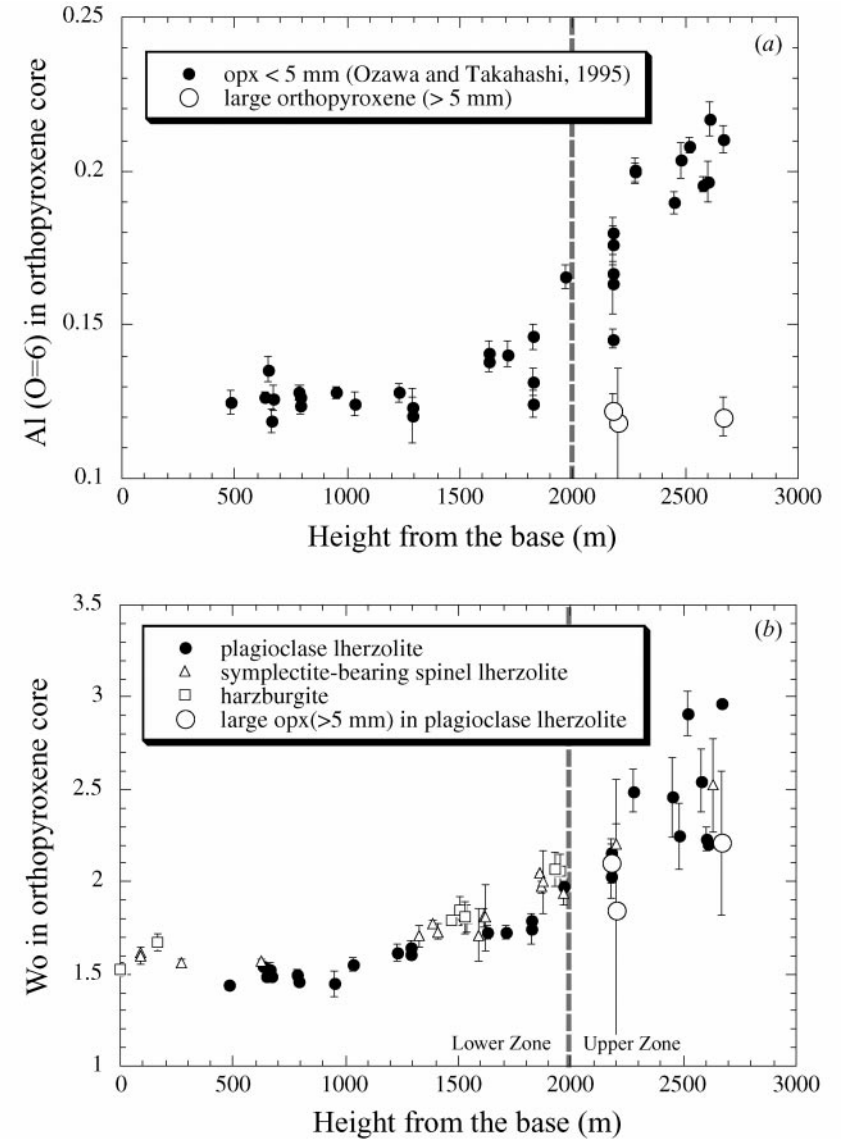

Fig. 7. Spatial variation of Al cations (O = 6) and %Wo in orthopyroxene cores in the Horoman peridotite complex. The data are plotted against height from the base calculated on the basis of the geological map of Niida (1974). Only the data from plagioclase lherzolites are plotted in the Al diagram, to eliminate bulk composition effect. ●, △ and □, orthopyroxene grains <5 mm (Fig. 2) after Ozawa & Takahashi (1995). ○, orthopyroxene crystals >5 mm (Fig. 2). All the analyses to obtain average core compositions were made with a defocused beam (20 μm). Each error bar for the new data represents the standard deviation of broad beam analyses in the core region of a megacryst, whereas that taken from the literature is the standard deviation of analyses on several porphyroclastic grains. The Ca content (O = 6) in orthopyroxene is approximately two times the Wo content.

and inter-mineral equilibrium in the fine-grained aggregates or rims of large crystals was reached only near the boundary of the spinel and plagioclase stability fields.

Two-pyroxene + spinel symplectite aggregates in orthopyroxene porphyroclasts in a plagioclase lherzolite sample from the Lower Zone also provide additional petrographic information on the latest *P–T* conditions. The spinel in this sample is very aluminous [Cr number = 100 × Cr/(Cr + Al) ~10], and there is no sign of reaction to form plagioclase. The occurrence of an intact two-pyroxene + spinel symplectite in an Na-depleted local environment (inclusion in orthopyroxene) in a plagioclase lherzolite suggests a significant temperature drop at a pressure in the vicinity of the boundary between plagioclase and spinel facies (Ozawa & Takahashi, 1995).

P–T trajectory of the Lower Zone

In the Lower Zone, orthopyroxene and clinopyroxene porphyroclasts in plagioclase lherzolite and

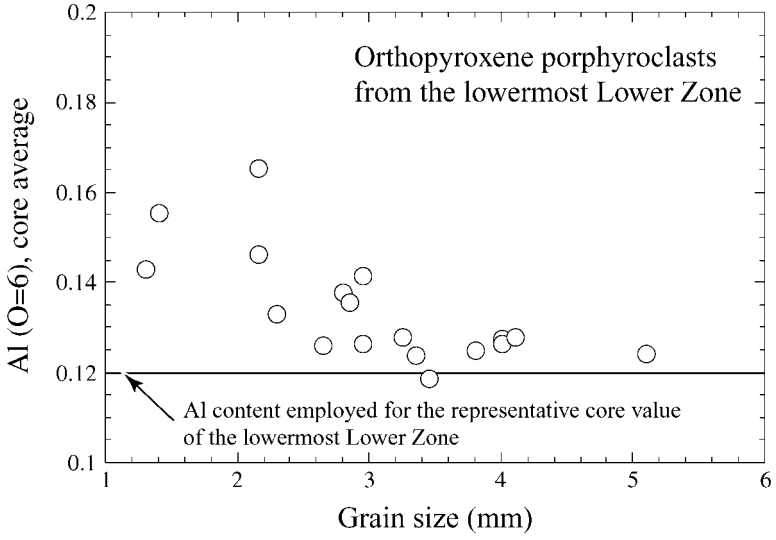

Fig. 8. Average Al cations (O = 6) plotted against the size of orthopyroxene porphyroclasts in plagioclase lherzolites from the lowest horizon of the Lower Zone of the Horoman complex. The horizontal line indicates the minimum value for the cores of orthopyroxene grains with ~5 mm size, which may be taken to represent the lowermost Lower Zone.

symplectite-bearing spinel lherzolite show Al zoning strongly dependent on grain size; large grains exhibit M-shaped Al zoning profiles, whereas smaller grains show Al contents monotonously decreasing from the core to the rim. The core Al content decreases with increase in grain size, and tends to attain a minimum value. In the lowermost horizon of the Lower Zone, a grain size of ~5 mm is enough to attain the minimum value of ~0·12 (Fig. 8). Large orthopyroxene porphyroclasts ~5 mm in size from the lowermost Lower Zone are homogeneous in terms of their Ca content [0·029 in Ca (O = 6) or 1·5 in Wo].

Because isolated spinel grains occurring outside fine-grained aggregates in plagioclase and symplectite-bearing spinel lherzolites from the Lower Zone are notably more Cr-rich and Al-rich, respectively, than spinel present in the fine-grained aggregates, the peridotites attain neither chemical nor textural equilibrium within the plagioclase and spinel facies. Moreover, the Al content of the cores is too low to be in equilibrium with other phases in the spinel stability field at the temperature indicated by the Ca content of the orthopyroxenes (<800°C vs >900°C). Therefore, it is concluded that the cores of the large orthopyroxene porphyroclasts with low and uniform Al contents record an equilibrium condition in the garnet stability field.

The temperature and pressure conditions of the lowermost Lower Zone in the garnet stability field before the start of ascent are constrained by the core Ca [0·03 ± 0·002 in Ca (O = 6) or 1·54 ± 0·09 in Wo after subtracting non-quadrilateral components] and Al contents in orthopyroxene [0·12 in Al (O = 6) or 6·7 ± 0·2% in Al(M1)*, Al (O = 6) in M1 site extrapolated to the Cr-free system] at 900 ± 20°C and 1·75 ± 0·07 GPa using a single pyroxene geothermobarometer combining the methods of Lindsley (1983) and Gasparik (1987) (Fig. 9). The errors are 1σ and were estimated from analyses of orthopyroxene cores >3·5 mm near the bottom of the Lower Zone. The lowest temperature and pressure conditions registered in the orthopyroxene rims are estimated by the same approach to be ~800°C and ~0·6 GPa (Fig. 9). Two-pyroxene or single-clinopyroxene geothermobarometry was not used for two reasons. First, clinopyroxene porphyroclasts commonly have more abundant and coarser exsolution and inclusions than orthopyroxene. Second, kinetic processes make it difficult to apply geothermobarometry based on more than one phase; it is necessary to decide which pairs are in equilibrium, but the existence of such pairs is not guaranteed.

Application of the Ca-in-orthopyroxene thermometer of Brey & Köhler (1990), which has been often used in the literature (e.g. Takazawa *et al.*, 1996), gives higher temperature by ~100°C and accordingly higher pressure by ~0·4 GPa than those estimated above. The discrepancy is basically due to the difference in treatment of Fe^{2+}, which increases the Ca solubility in orthopyroxene coexisting with clinopyroxene (Lindsley, 1983; Sack & Ghiorso, 1994). This effect is ignored in the thermometry of Brey & Köhler (1990), who argued that the higher Al content in natural system compensates for the Fe effect. Perkins & Newton (1980) demonstrated that the mutual solubility of pyroxenes widens (decrease in Ca for orthopyroxene) in the Al-bearing system by comparing experiments in the CMS and CMAS systems. Experimental results in the CMS and CMAS systems (Perkins & Newton, 1980; Nickel & Brey, 1984; Nickel *et al.*, 1985) show that the Al effect is more notable at low pressure <3 GPa. Within this

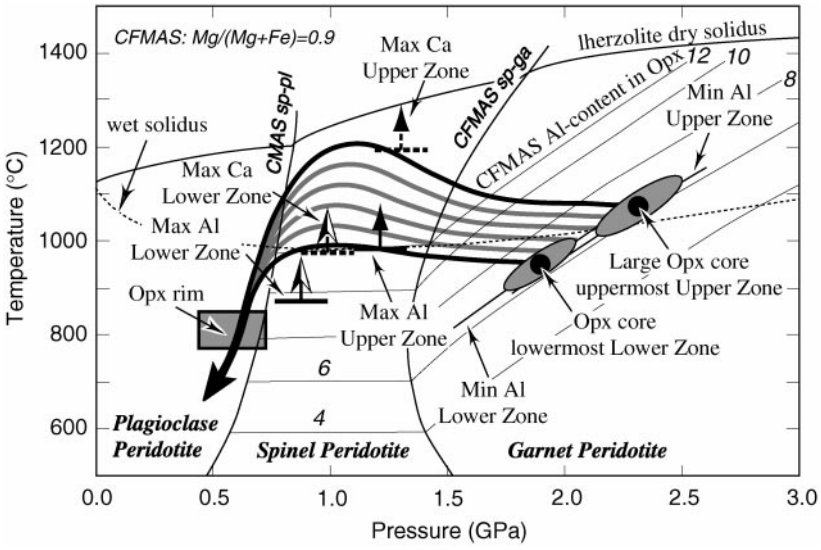

Fig. 9. Temperature and pressure constraints for the thermal history of the Upper and Lower Zones of the Horoman complex and inferred P–T trajectories. The P–T trajectories for the lowermost Lower Zone and the uppermost Upper Zone, shown by thick black curves, are inferred on the basis of the Al and Ca orthopyroxene zoning in plagioclase lherzolites. The thick gray curves between the black curves indicate that the P–T paths vary continuously within the complex. The ascent paths start from the P–T estimation (●) based on the core compositions of very large orthopyroxene megacrysts (>5 mm). The grey shaded ellipses for each zone represent the uncertainty in the P–T estimation [Ca and minimum Al contents in the cores according to Lindsey (1983) and Gasparik (1987) after modification of the Al effect; see text for more detail]. The P–T paths in the spinel stability field are constrained by the maximum Ca and Al contents registered in the marginal zones (or cores of small grains) in the plagioclase lherzolites of the Upper Zone and Lower Zone, respectively. The paths in the plagioclase stability field are constrained by the Ca and Al contents of orthopyroxene rims, in addition to the presence of plagioclase in fertile lherzolites. Facies boundaries for peridotite and isopleths of Al content in orthopyroxene (thin black lines) in the Ca–Fe–Mg–Al–Si system are after Gasparik (1987). The facies boundary of the plagioclase and spinel peridotite stability field is for the Ca–Mg–Al–Si system and that for spinel and garnet peridotites is for the Ca–Fe–Mg–Al–Si system with Mg/(Mg + Fe) = 0·9 (Gasparik, 1987). In the Cr-bearing system the spinel stability field is wider than that shown in this figure (Green & Hibberson, 1970; O'Neill, 1981). The dry lherzolite solidus is after Takahashi & Kushiro (1986). The wet solidus after Kushiro *et al.* (1968).

range of pressure, however, the decrease in Ca content (O = 6) in the CMAS system in the presence of garnet relative to the CMS system is <0·004 on average, which is far below the difference of 0·015 caused by a change in Mg number [100 × Mg/(Mg + Fe)] from 90 to 100. This Al effect corresponds to a rise in temperature by 50°C on average for the same Ca content at pressures <3 GPa and temperatures ranging from 900 to 1100°C, although the estimation contains significant errors because of the limited numbers of experiments and less tight bracketing (Nickel & Brey, 1984; Nickel *et al.*, 1985). Application of this temperature correction to the above estimation yields ∼950°C and ∼1·9 GPa as the equilibrium conditions for the lowermost Lower Zone before the Horoman complex started to ascend.

The Fe effect is more significant than that of Lindsley (1983) in the quadrilateral pyroxene system thermodynamically calibrated by Sack & Ghiorso (1994), and gives temperatures lower by ∼50°C and pressure lower by ∼0·2 GPa than those estimated above (∼900°C and 1·75 GPa after correcting for the Al effect).

The Ca zoning in orthopyroxene porphyroclasts suggests a nearly adiabatic P–T trajectory for the lowermost Lower Zone. Orthopyroxene often shows a marginal hump in its Ca content higher than the core region by up to 0·007 (0·2 in Wo), which represents the minimum estimate for the peak temperature during decompression. The Ca zoning implies an isothermal trajectory (or a slight temperature rise) during the decompression because the isopleths for Ca in orthopyroxene with Mg number 91 are 0·002–0·004/GPa (0·1–0·22/GPa in Wo) at a temperature in the range of 800–1000°C (Sack & Ghiorso, 1994). Because of the constraint from the P–T condition recorded in the rim of orthopyroxene porphyroclasts (∼800°C, ∼0·6 GPa), there should be a rapid fall in temperature within a small decrease of pressure at a shallower level (Fig. 9).

Such a P–T trajectory is consistent with the M-shaped Al zoning in orthopyroxene as shown by Ozawa (1997), who modeled the development of Al zoning in orthopyroxene during decompression of peridotite (Fig. 10; see Appendix for details of modeling). The M-shaped zoning pattern can be formed when the decompression path is nearly isothermal from the garnet stability field to the boundary of the plagioclase and spinel fields after which temperature falls rapidly (Figs 9 and 10a). For grain size of ∼5 mm, the largest porphyroclasts in the Lower Zone, and a decompression rate of 1 kPa/year, no marginal peak in Al is produced if the P–T trajectory is too steep (paths 9–13 in Fig. 10a and b). Furthermore, only a very

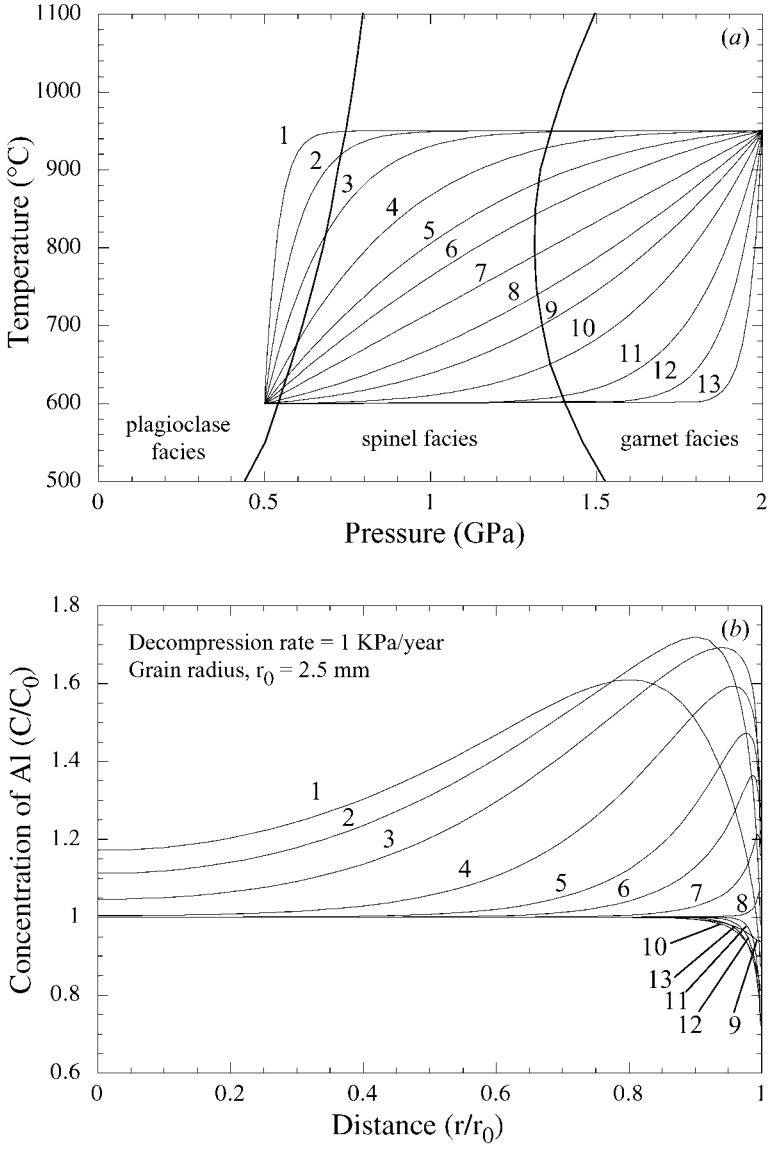

Fig. 10. Frozen Al zoning profiles (b) for ascent from 2·0 GPa and 950°C at a constant decompression rate along the *P–T* trajectories shown in (a). Numbers in (b) correspond to the marked *P–T* paths in (a). The thick curves in (a) represent the boundaries between the plagioclase and spinel stability fields and between the spinel and garnet stability fields. The Al concentration is normalized to the initial value and plotted vs distance from the center normalized to the radius of the grain in (b). (See Appendix for the model calculation and its assumptions.)

minor marginal peak is produced if the temperature fall at high pressure is significant, because rapid cooling restrains diffusion of Al into the marginal zone from the surface with high Al content (paths 6–8 in Fig. 10a and b). *P–T* trajectories that reproduce the typical M-shaped Al zoning must have a gentler slope in the *P–T* diagram (e.g. paths 1–5 in Fig. 10a and b).

Because the Al zoning pattern strongly depends on the decompression rate, the ascent rate can be determined by simulating the zoning profile if reliable Al diffusivity data in orthopyroxene are available (Fig. 11). Available Al diffusivity data (Smith & Barron, 1991) give ~1 kPa/year for the ascent rate with three constraints: the presence of a marginal Ca hump, the ratio of Al content in the marginal zone against that of the core <1·5, and the preservation of a wide region with constant Al content in the center (Fig. 8). To fulfill the second constraint, a steeper *P–T* path such as path 4 in Fig. 10 is more plausible, but this cannot be consistent with the first constraint requiring nearly isothermal conditions.

The observed lower marginal maximum in Al content than expected from Fig. 11 is attributable to a decrease in decompression rate at a pressure of ~0·6 GPa, where the Horoman complex encountered the Hidaka crust

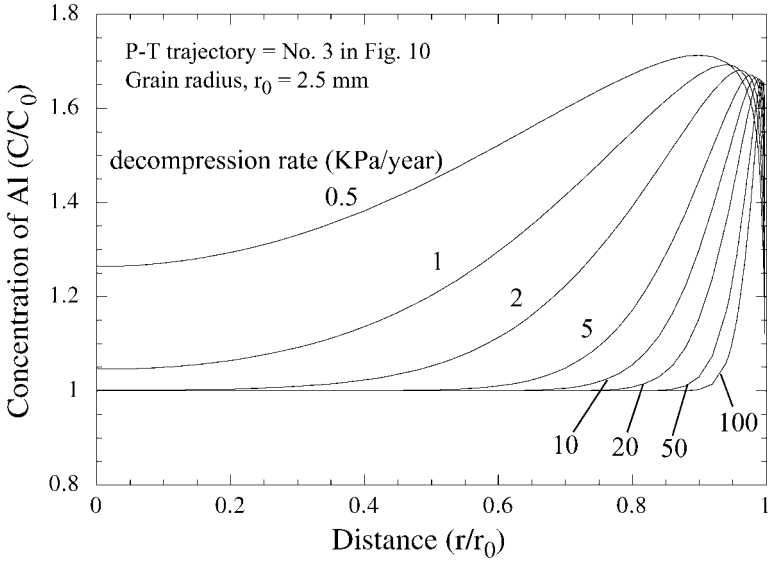

Fig. 11. Frozen-in Al profiles for ascent processes from 2·0 GPa and 950°C at various constant decompression rates along *P–T* trajectory 3 shown in Fig. 10a. Numbers indicate decompression rate in kPa/year. The Al concentration is normalized to the initial value and plotted against distance from the center normalized to the radius of the grain.

(Ozawa, 1997). The estimated rate has large errors (probably more than one order of magnitude) because the diffusivity data obtained from Al zoning in natural orthopyroxene in contact with garnet contain large uncertainties, so they must be viewed with caution. The assumption of a constant decompression rate also introduces an additional uncertainty into the rate estimated above.

P–T history of the Upper Zone

In deriving the thermal history of the Upper Zone, previous investigators assumed that the core compositions of the orthopyroxene porphyroclasts represent that of the garnet stability field. Ozawa (1997), however, pointed out that the high Al and Ca contents in orthopyroxene porphyroclasts in the Upper Zone can also be explained by a heating event at ~1 GPa during ascent from an initial condition similar to that of the Lower Zone (~950°C and ~2·0 GPa). He examined this possibility in detail by forward modeling of Al zoning in orthopyroxene during ascent of plagioclase lherzolite for various *P–T* paths and decompression rates (see Appendix for modeling details).

One set of decompression paths examined by Ozawa (1997) is shown in Fig. 12. One of these is similar to the *P–T* trajectory inferred for the lowermost Lower Zone and features an isothermal decompression path followed by a rapid temperature drop in the plagioclase stability field (path 9). Other trajectories (paths 1–8) are those for a heating event in the spinel stability field for various heating duration starting from the same *P–T* conditions in the garnet stability field as that of path 9. The decompression paths 5–9 qualitatively reproduce the Al zoning in porphyroclastic orthopyroxene with grain size less than 5 mm from the Lower Zone, and paths 1–3 reproduce that of the Upper Zone. The heating model is coherent with the notable marginal hump in Ca content in orthopyroxene and the corresponding marginal minimum for Ca content in clinopyroxene commonly observed in the Upper Zone. Pyroxene megacrysts, for which data are presented above, provide critical information to substantiate the suggestion that the Upper Zone actually experienced a heating event.

The core Al content in the orthopyroxene megacrysts from the Upper Zone is significantly lower than that of the porphyroclasts (<5 mm in size) in the plagioclase lherzolites of the Upper Zone (Fig. 7a). The Al content of the orthopyroxene megacryst cores is nearly constant in the Upper Zone. The core Ca content in the orthopyroxene megacrysts is lower than that of the porphyroclasts, and shows a slight increase with stratigraphic height in the Upper Zone (Fig. 7b). The variation in the composition of the porphyroclasts within the complex as a whole is continuous without any gap between the two zones. The presence of wide core regions with fairly homogeneous composition for orthopyroxene (Figs 3 and 4) and clinopyroxene (Figs 5 and 6) suggests that the core compositions represent meaningful initial conditions at which the Horoman peridotites stayed for a fairly long time. The occurrence of pyroxene megacrysts in a thin plagioclase-rich layer <1 cm in thickness, surrounded by plagioclase lherzolite with the typical grain size, mineral mode and texture suggests that the megacrysts could have been in equilibrium with minerals in the host lherzolite in the garnet stability field.

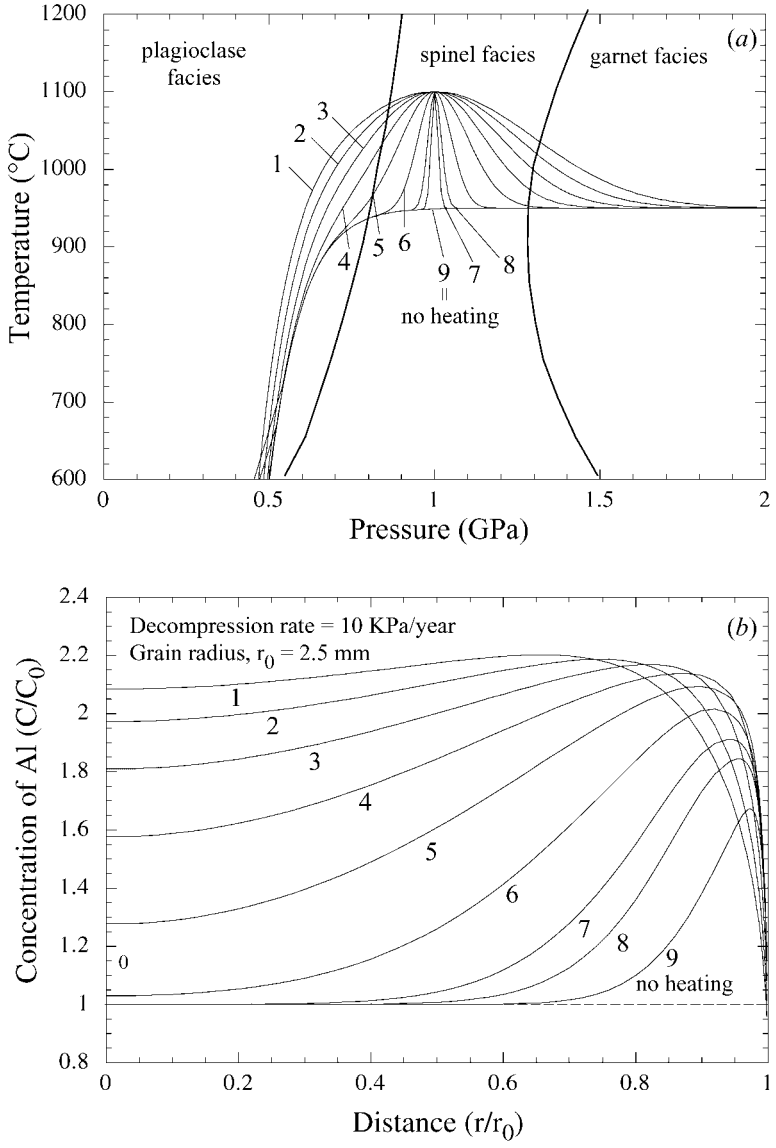

Fig. 12. Frozen-in Al zoning profiles (b) modeled for ascent of a fertile lherzolite from 2·0 GPa and 950°C at a constant decompression rate along several P–T trajectories with heating stages as shown in (a). The heating paths 1–8 differ in heating duration (or depth range of heating). The thick curves in (a) represent the boundaries between the plagioclase and spinel stability fields and between the spinel and garnet stability fields. The Al concentration in (b) is normalized to the initial value and plotted vs distance from the center normalized to the radius of the grain.

After correcting for the Al effect, the equilibrium conditions are estimated to be 1070 ± 30°C and 2·3 ± 0·11 GPa for the uppermost Upper Zone based on 0·042 ± 0·004 in Ca (O = 6) (Wo = 2·2 ± 0·2) and 0·12 in Al (O = 6) [Al(M1)* = 6·22%; Table 3]. Because only one megacryst was analyzed at each locality, the maximum errors for porphyroclastic grains <5 mm in size are employed. These P–T conditions are obviously higher than those of the lowermost Lower Zone.

A maximum Al (O = 6) content in the marginal zone of the orthopyroxene megacrysts as high as 0·2 [~12% in Al(M1)*; Fig. 4] can be explained by a nearly adiabatic decompression path. However, the maximum Ca content in the marginal zone attains 0·065 (0·033 in Wo; Fig. 4), which is similar to the Ca contents of smaller orthopyroxene cores from the uppermost Upper Zone (Fig. 3). These high Ca contents correspond to ~1200°C at 1·0 GPa, suggesting that the Upper Zone experienced a heating event in the spinel stability field with a temperature rise of ~130°C (Fig. 9). Application of the Ca-in-orthopyroxene thermometer of Brey & Köhler (1990) gives a much smaller temperature rise of ~70°C.

Implication of the variation in the 'initial *P–T* conditions' in the Horoman peridotite complex

The *P–T* estimated conditions in the garnet stability field for the lowermost Lower Zone and the uppermost Upper Zone, based on orthopyroxene geothermobarometry, differ by 120 ± 50°C and 0·4 ± 0·18 GPa. Because the Al contents of the cores of the large orthopyroxenes are similar, the variation in the estimated conditions is principally attributable to the Ca content, the difference of which is statistically significant [0·03 ± 0·002 vs 0·042 ± 0·004 in Ca (O = 6) and 1·54 ± 0·09 vs 2·2 ± 0·2 in Wo; Fig. 7]. Although the absolute *P–T* estimates can vary by 150°C and 0·5 GPa depending on the applied geothermometers, the temperature difference is similar for any of the geothermometers.

Comparing the 'initial conditions' in the garnet stability field for the two zones, it is suggested that the Horoman complex was originally a part of the lithospheric upper mantle with the Lower Zone overlying the Upper Zone. A temperature gradient existed in the Horoman mantle, although the variation may not have been as large as that suggested by Ozawa & Takahashi (1995). The estimated vertical temperature gradient within the Horoman mantle is ∼10 ± 8°C/km. This value is comparable with the geothermal gradient in the lithospheric mantle estimated by applying geothermobarometers to lherzolite xenoliths (4–6°C/km; Boyd, 1973; Rudnick & Nyblade, 1999; Nimis & Taylor, 2000) if the large error is taken into consideration. It may represent the thermal gradient of the Horoman lithospheric upper mantle. If the pressure difference between the two zones is accepted, the distance between the top of the Upper Zone and the basal part of the Horoman complex is estimated to be 12 ± 5 km, which is much greater than the current thickness of the Horoman complex (∼3 km), by a factor of 4 ± 2. This can be interpreted as stretching that the Horoman complex underwent during its emplacement into the Hidaka lower crust.

Origin of the Upper and Lower Zones and its relevance to the thermal history

Table 1 summarizes geological, petrographic and mineralogical contrasts between the Upper and Lower Zones, compiled from previous studies of the Horoman complex (see references in the table legend). Any comprehensive model for the origin of the Horoman complex must explain all these features. A variable thermal history within the Horoman complex can account for most of the observed differences.

The higher-temperature path followed by the Upper Zone, irrespective of the exact ascent *P–T* path, can explain most of the petrographic and mineralogical distinctions. For example, the larger grain size of the two-pyroxene spinel symplectites and fine-grained aggregates after the symplectites in the Upper Zone peridotites can be attributable to rapid grain growth during a prolonged higher-temperature stage, assuming comparable strain rates. The more homogeneous composition of plagioclase and spinel in the Upper Zone peridotites can be explained by rapid elemental diffusion in the minerals and also along grain boundaries because of the high-temperature ascent path. The minor occurrence of symplectite-bearing spinel lherzolite in the Upper Zone may be partly attributable to more enhanced subsolidus reaction to produce plagioclase in the symplectite-bearing spinel lherzolites.

Ozawa & Takahashi (1995) argued that the Upper Zone might have partially melted where enough water was available. They further speculated that the plagioclase-rich veins oblique to the foliation were fractures filled by melt segregated from the surrounding partially molten peridotite (segregation veins; Table 1). Takahashi (2001) reported abundant plagioclase-rich segregation veins and also oscillatory Ca–Na growth zoning of plagioclase in the plagioclase lherzolites of the Nikanbetsu complex. These observations provide unequivocal evidence for partial melting and minor segregation in the Nikanbetsu complex, which is the high-temperature extremity of the Upper Zone of the Horoman complex. Therefore, it is plausible that the Upper Zone also underwent partial melting, and some of the geological contrasts with the Lower Zone (Table 1) may also be attributed to this melting event.

Isotopic ages for the mafic rocks (Takazawa *et al.*, 1999) and peridotites (Yoshikawa & Nakamura, 2000) indicate that the mafic layers and the major lithological variation shown by the peridotites were not formed during the final ascent of the complex. The preservation of such old geological structures consistently overlapping the younger thermal structure can be explained by the overturned stratification of the two zones. The initially hotter and deeper Upper Zone may represent a lower part of the lithospheric mantle that now overlies the Lower Zone, which was a cooler and shallower part of the lithospheric mantle (Ozawa, 1997). Sawaguchi (2001) proposed that the current sequence of stratification within the Horoman complex could be explained by inverted thermal structures in the mantle wedge above a subducting slab. However, the estimated *P–T* conditions within the garnet stability field negate this possibility.

Implication of the difference in ascent *P–T* path between the two zones

The petrographical and mineralogical observations on the Horoman complex may indicate that the upper part of the complex experienced a heating event in the spinel

stability field during its ascent from the garnet stability field, and that the lowest part of the complex ascended almost adiabatically. The continuous variations of Ca and Al contents in orthopyroxene within the complex (Fig. 7) indicate that a thermal gradient was maintained up to the boundary between the spinel and plagioclase lherzolite stability fields.

The source of heat for the inferred heating event could be basaltic melt, which might be responsible for the formation of gabbroic rocks within the Hidaka metamorphic belt (Maeda & Kagami, 1996), passing through the Upper Zone itself or a region more closely adjacent to the Upper Zone than to the Lower Zone. Another possibility is that heating was induced by a hot asthenospheric, mantle diapir which was emplaced into the lithosphere adjacent to the Upper Zone (Van der Wal & Vissers, 1993; Kimura, 1996; Model 2 of Ozawa, 1997; Drury *et al.*, 2001). Because the Upper Zone currently occupies the upper part of the complex, the sequence must have been overturned by the quicker ascent of the hotter, deeper part associated with heating. Overturning of the heated part cannot be caused only by magma ascent through fractures, and the hot ascending diapir model seems much more plausible (Ozawa, 1997). The hot Horoman complex itself might have acted as a significant heat source when it was emplaced into the lower crust of the Hidaka metamorphic belt, where it triggered metamorphism and partial melting of the lower-crustal rocks (Tagiri *et al.*, 1995).

CONCLUSIONS

The thermal history of the Horoman peridotite complex proposed by Ozawa & Takahashi (1995) has been revised based on newly obtained data for the Ca and Al contents of pyroxene megacrysts from the Upper Zone. The variation in Al content of the cores of large orthopyroxene megacrysts in the Upper Zone is notably different from their predicted values; the Al content is almost constant or decreases slightly from the bottom to the top of the Upper Zone. The revised variation of the Ca content in the largest (megacrysts and porphyroclasts) orthopyroxene cores exhibits a linear increase upwards from the middle of the Lower Zone, beneath which the Wo content is nearly constant. These variations in mineral chemistry suggest that the structurally higher horizons (Upper Zone) of the complex initially resided at higher temperature and pressure conditions (1070 ± 30°C, 2·3 ± 0·11 GPa) than the lower horizon (Lower Zone; 950 ± 20°C, 1·9 ± 0·07 GPa) before ascent from the garnet stability field.

The higher Ca contents of the cores of porphyroclasts with ~5 mm grain size than that of the megacrysts indicates that the Upper Zone experienced a heating event during its ascent through the spinel stability field, with peak temperatures higher than 1200°C. The effect of the heating event appeared to have decreased continuously toward the base of the complex, and the lower part of the Lower Zone underwent only a very minor heating event.

The thermal structure in the Horoman lithospheric mantle before the final decompression is comparable with that of the continental lithosphere. The vertical thermal gradient is estimated to be 10 ± 8°C/km. The current thickness of the Horoman complex (~3 km) is a result of flattening by factor of 0·25 ± 0·1 during its ascent from depth; this deformation was probably driven by the ascent of an asthenospheric mantle diapir.

ACKNOWLEDGEMENTS

Discussions with M. Obata, E. Takazawa and T. Sawaguchi during the Samani conference and on many other occasions were very helpful. I thank H. Nagahara for her encouragement and critically reading the manuscript, and E. Nakamura for stimulating discussion on the Horoman complex. Reviews by R. Altherr and two anonymous reviewers are greatly appreciated.

REFERENCES

Boyd, F. R. (1973). A pyroxene geotherm. *Geochimica et Cosmochimica Acta* **37**, 2533–2546.

Brenker, F. E. & Brey, G. P. (1997). Reconstruction of the exhumation path of the Alpe Arami garnet-peridotite body from depths exceeding 160 km. *Journal of Metamorphic Geology* **15**, 581–592.

Brey, G. P. & Köhler, T. (1990). Geothermobarometry in four-phase lherzolites II. New thermobarometers and practical assessment of existing thermobarometers. *Journal of Petrology* **31**, 1353–1378.

Carslaw, H. S. & Jaeger, J. C. (1959). *Conduction of Heat in Solids*. New York: Oxford University Press, 510 pp.

Davies, G. R., Nixon, P. H., Pearson, D. G. & Obata, M. (1993). Tectonic implications of graphitized diamonds from the Ronda peridotite massif, southern Spain. *Geology* **21**, 471–474.

Drury, M. R., van Roermund, H. L. M., Carswell, D. A., de Smet, J. H., van den Berg, A. P. & Vlaar, N. J. (2001). Emplacement of deep upper-mantle rocks into cratonic lithosphere by convection and diapiric upwelling. *Journal of Petrology* **42**, 1131–1140.

Gasparik, T. (1985). Experimental study of subsolidus phase relations and mixing properties of clinopyroxene and plagioclase in the system Na_2O–CaO–Al_2O_3–SiO_2. *Contributions to Mineralogy and Petrology* **89**, 346–357.

Gasparik, T. (1987). Orthopyroxene thermobarometry in simple and complex systems. *Contributions to Mineralogy and Petrology* **96**, 357–370.

Green, D. H. & Hibberson, W. (1970). The instability of plagioclase in peridotite at high pressure. *Lithos* **3**, 209–221.

Kadarusman, A. & Parkinson, C. D. (2000). Petrology and *P–T* evolution of garnet peridotites from central Sulawesi, Indonesia. *Journal of Metamorphic Petrology* **18**, 193–209.

Kimura, G. (1996). Collision orogeny at arc–arc junctions in the Japanese Islands. *Island Arc* **5**, 262–275.

Kitayama, I., Parkinson, C. D., Okamoto, K., Nakajima, Y. & Maruyama, S. (2000). Supersilicic clinopyroxene and silica

exsolution in UHPM eclogite and pelitic gneiss from the Kokchetav massif, Kazakhstan. *American Mineralogist* **85**, 1368–1374.

Komatsu, M. & Nochi, M. (1966). Ultrabasic rocks in the Hidaka metamorphic belt, Hokkaido, Japan. I. Mode of occurrence of the Horoman ultrabasic rocks. *Chikyukagaku* (*Earth Science*) **87**, 21–29.

Komatsu, M., Miyashita, S., Maeda, J., Osanai, Y. & Toyoshima, T. (1983). Disclosing of a deepest section of continental-type crust upthrust as the final event of collision of arcs in Hokkaido, North Japan. In: Hashimoto, M. & Uyeda, S. (eds) *Acccretion Tectonics in the Circum-Pacific Regions*, Tokyo: TERRAPUB, pp. 149–165.

Kornprobst, J. (1969). Le massif ultrabasique des Beni Bouchera (Rif Interne, Maroc): étude des peridotites de haute température et de haute pression, et des pyroxénolites, à grenat ou sans grenat, qui leur sont associées. *Contributions to Mineralogy and Petrology* **23**, 288–322.

Kushiro, I. & Yoder, H. S. (1966). Anorthite–forsterite and anorthite–enstatite reactions and their bearing on the basalt–eclogite transformation. *Journal of Petrology* **7**, 337–362.

Kushiro, I., Syono, Y. & Akimoto, S. (1968). Melting of a peridotite nodule at high pressures and high water pressures. *Journal of Geophysical Research* **73**, 6023–6029.

Lasaga, A. C. (1983). Geospeedometry: an extension of geothermometry. In: Saxena, S. K. (ed.) *Kinetics and Equilibrium in Mineral Reactions, Vol. 3: Advances in Physical Geochemistry*. New York: Springer, pp. 81–114.

Lindsley, D. H. (1983). Pyroxene thermometry. *Amrican Mineralogist* **68**, 477–493.

Loubet, M. & Allègre, C. J. (1979). Trace element studies in the Alpine type peridotite of Beni-Bouchera (Morocco). *Geochemical Journal* **13**, 69–75.

MacGregor, I. D. & Basu, A. R. (1976). Geological problems in estimating mantle geothermal gradients. *American Mineralogist* **61**, 715–724.

Maeda, J. & Kagami, H. (1996). Interaction of a spreading ridge and an accretionary prism: implications from MORB magmatism in the Hidaka magmatic zone, Hokkaido, Japan. *Geology* **24**, 31–34.

Nickel, K. G. & Brey, G. (1984). Subsolidus orthopyroxene–clinopyroxene systematics in the system CaO–MgO–SiO_2 to 60 kb: a re-evaluation of the regular solution model. *Contributions to Mineralogy and Petrology* **87**, 35–42.

Nickel, K. G., Brey, G. P. & Kogarko, L. (1985). Orthopyroxene–clinopyroxene equilibria in the system CaO–MgO–Al_2O_3–SiO_2 (CMAS): new experimental results and implications for two-pyroxene thermometry. *Contributions to Mineralogy and Petrology* **91**, 44–53.

Nicolas, A. (1989). *Structures of Ophiolites and Dynamics of Oceanic Lithosphere*. Dordrecht: Kluwer Academic.

Niida, K. (1974). Structure of the Horoman ultramafic massif of the Hidaka metamorphic belt in Hokkaido, Japan. *Journal of Geological Society of Japan* **80**, 31–44.

Niida, K. (1975). Textures and olivine fabrics of the Horoman ultramafic rocks, Japan. *Journal of Mineralogy, Petrology and Economic Geology* **70**, 265–285.

Niida, K. (1984). Petrology of the Horoman ultramafic rocks in the Hidaka metamorphic belt, Hokkaido, Japan. *Journal of Faculty of Sciences, Hokkaido University, Series IV* **21**, 197–250.

Niida, K. & Katoh, T. (1978). Ultramafic rocks in Hokkaido. *Monograph of Association for Geological Collaboration in Japan* **21**, 61–81 (in Japanese with English abstract).

Nimis, P. & Taylor, W. R. (2000). Single clinopyroxene thermobarometry for garnet peridotites. Part I. Calibration and testing of a Cr-in-Cpx barometer and an enstatite-in-Cpx thermometer. *Contributions to Mineralogy and Petrology* **139**, 541–554.

Nimis, P. & Trommsdorff, V. (2001). Comment on new constraints on the *P–T* evolution of the Alpe Arami garnet peridotite body (central Alps, Switzerland) by Paquin & Altherr (2001). *Journal of Petrology* **42**, 1773–1779.

Obata, M. (1980). The Ronda peridotite: garnet-, spinel-, and plagioclase-lherzolite facies and the *P–T* trajectories of a high temperature mantle intrusion. *Journal of Petrology* **21**, 533–572.

Obata, M. & Nagahara, K. (1997). Layering of Alpine-type peridotite and the segregation of partial melt in the upper mantle. *Journal of Geophysical Research* **92**, 3467–3474.

Obata, M., Morisita, R. & Tanaka, K. (1997). The microstructure of symplectite in the Horoman peridotite and its formation processes. *Memoir of the Geological Society of Japan* **47**, 163–171 (in Japanese with English abstract).

O'Neill, H. S. C. (1981). The transition between spinel lherzolite and garnet lherzolite, and its use as a geobarometer. *Contributions to Mineralogy and Petrology* **77**, 185–194.

Ozawa, K. (1997). *P–T* history of an ascending mantle peridotite constrained by Al zoning in orthopyroxene: a case study in the Horoman peridotite complex, Hokkaido, northern Japan. *Memoir of the Geological Society of Japan* **47**, 107–122.

Ozawa, K. & Takahashi, N. (1995). *P–T* history of a mantle diapir: the Horoman peridotite complex, Hokkaido, northern Japan. *Contributions to Mineralogy and Petrology* **120**, 223–248.

Paquin, J. & Altherr, R. (2001*a*). New constraints on the *P–T* evolution of the Alpe Arami garnet peridotite body (central Alps, Switzerland). *Journal of Petrology* **42**, 1119–1140.

Paquin, J. & Altherr, R. (2001*b*). 'New constraints on the *P–T* evolution of the Alpe Arami garnet peridotite body (central Alps, Switzerland)': Reply to comment by Nimis & Trommsdorff (2001). *Journal of Petrology* **42**, 1781–1787.

Perkins, D., III & Newton, R. C. (1980). The compositions of coexisting pyroxenes and garnet in the system CaO–MgO–Al_2O_3–SiO_2 at 900°C–1100°C and high pressures. *Contributions to Mineralogy and Petrology* **75**, 291–300.

Rudnick, R. L. & Nyblade, A. A. (1999). The thickness and heat production of Archean lithosphere: constraints from xenolith thermobarometry and surface heat flow. In: Fei, Y., Bertka, C. M. & Mysen, B. O. (eds) *Mantle Petrology: Field Observations and High Pressure Experimentation, A Tribute to Francis R. (Joe) Boyd. Geochemical Society Special Publication* **6**, 3–12.

Sack, R. O. & Ghiorso, M. S. (1994). Thermodynamics of multicomponent pyroxenes: II. Phase relations in the quadrilateral. *Contributions to Mineralogy and Petrology* **116**, 287–300.

Sawaguchi, T. (2001). Structural petrology of the Horoman peridotite: deformation history and exhumation process of the Alpine-type peridotite massif. Ph.D. thesis, Waseda University.

Sawaguchi, T. & Takagi, H. (1997). Inverted ductile shear movement of the Horoman peridotite complex in the Hidaka metamorphic belt, Hokkaido, Japan. *Memoir of the Geological Society of Japan* **47**, 193–208.

Smith, D. & Barron, B. R. (1991). Pyroxene–garnet equilibration during cooling in the mantle. *American Mineralogist* **76**, 1950–1963.

Tagiri, M., Tanaka, H. & Shiba, M. (1995). Melting of amphibolites and the form of melt-trap in amphibolite–migmatites of the southern Hidaka metamorphic belt, Hokkaido, Japan. *Journal of Mineralogy, Petrology and Economic Geology* **90**, 50–63.

Takahashi, E. & Kushiro, I. (1986). Melting of a dry peridotite at high pressure and basalt magma genesis. *American Mineralogist* **68**, 859–879.

Takahashi, N. (1991). Origin of three peridotite suite from Horoman peridotite complex, Hokkaido, Japan; melting, melt segregation and solidification processes in the upper mantle. *Journal of Mineralogy, Petrology and Economic Geology* **86**, 199–215.

Takahashi, N. (1992). Evidence for melt segregation towards fractures in the Horoman mantle peridotite complex. *Nature* **359**, 52–55.

Takahashi, N. (1997). Incipient melting of mantle peridotites observed in the Horoman and Nikanbetsu peridotite complexes, Hokkaido, northern Japan. *Journal of Mineralogy, Petrology and Economic Geology* **92**, 1–24.

Takahashi, N. (2001). Origin of plagioclase lherzolite from the Nikanbetsu peridotite complex, Hokkaido, northern Japan: implications for incipient melt migration and segregation in the partially molten upper mantle. *Journal of Petrology* **42**, 39–54.

Takahashi, N. & Arai, S. (1989). Textural and chemical features of chromian spinel pyroxene symplectite in the Horoman peridotites, Hokkaido, Japan. *Scientific Report of Institute of Geosciences of University of Tsukuba, Section B* **10**, 45–55.

Takazawa, E., Frey, F., Shimizu, N. & Obata, M. (1996). Evolution of the Horoman peridotite (Hokkaido, Japan): implications from pyroxene compositions. *Chemical Geology* **134**, 3–26.

Takazawa, E., Frey, F. A., Shimizu, N., Saal, A. & Obata, M. (1999). Polybaric petrogenesis of mafic layers in the Horoman peridotite complex, Japan. *Journal of Petrology* **40**, 1827–1851.

Tazaki, K., Ito, E. & Komatsu, M. (1972). Experimental study on a pyroxene–spinel symplectite at high pressures and temperatures. *Journal of Geological Society of Japan* **78**, 347–354.

Tsai, C.-H., Liou, J. G. & Erns, W. G. (2000). Petrological characterization and tectonic significance of retrogressed garnet peridotites, Raobazhai area, North Dabie Complex, east–central China. *Journal of Metamorphic Geology* **18**, 181–192.

Tubía, J. M. (1994). The Ronda peridotites (Los Reales nappe): an example of the relationship between lithospheric thickening by oblique tectonics and late extensional deformation within the Betic Cordillera (Spain). *Tectonophysics* **238**, 381–398.

Van der Wal, D. & Vissers, R. L. M. (1993). Uplift and emplacement of upper mantle rocks in the western Mediterranean. *Geology* **21**, 1119–1122.

Van Roermund, H. L. M., Drury, M. R., Barnhoorn, A. & de Ronde, A. A. (2000). Super-silicic garnet microstructures from an orogenic garnet peridotite, evidence for an ultra-deep (>6 GPa) origin. *Journal of Metamorphic Geology* **18**, 135–147.

Yang, J., Godard, G., Kienast, J.-R., Lu, Y. & Sun, J. (1993). Ultrahigh-pressure (60 kbar) magnesite-bearing garnet peridotites from northeastern Jiangsu, China. *Journal of Geology* **101**, 541–554.

Yoshikawa, M. & Nakamura, E. (2000). Geochemical evolution of the Horoman peridotite complex: implications for melt extraction, metasomatism, and compositional layering in the mantle. *Journal of Geophysical Research* **105**, 2879–2901.

APPENDIX: KINETIC MODEL FOR Al ZONING IN ORTHOPYROXENE PORPHYROCLASTS

To model Al zoning of orthopyroxene in the peridotite system, we have to simplify the reaction processes, which involve transportation through grain boundaries, diffusion in an orthopyroxene grain, and migration of grain surface. If peridotites have porphyroclastic or mylonitic textures, consisting of a small number of large pyroxene crystals and a dominant fine-grained matrix, we can simplify the reaction system as illustrated in Fig. A1. In this case, we can divide the system into two domains: an equilibrium domain (matrix), in which the minerals are nearly in equilibrium because of their smaller grain size, and a kinetically controlled domain (porphyroclasts), in which the minerals cannot attain equilibrium because of their larger grain size. Rapid reactions involving net mass-transfer between the minerals in the fine-grained matrix suppress grain growth or dissolution of large porphyroclasts, which communicate with the fine-grained matrix at a rate limited by lattice diffusion in the porphyroclasts. The matrix may contain large minerals, such as garnet, but this does not affect the behaviour of two domains unless diffusion in such minerals affects the overall reaction rate in the equilibrium domain.

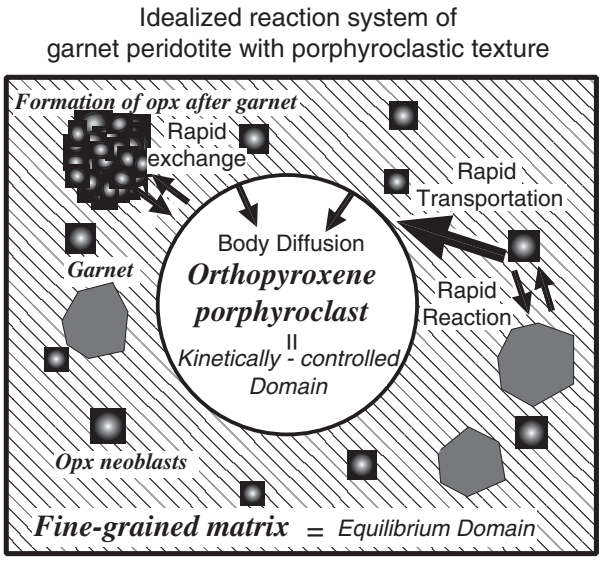

Fig. A1. Schematic illustration of the reaction model employed in this paper to model the Al zoning in orthopyroxene during decompression of lherzolite from the garnet stability field (Ozawa, 1997). Only the large orthopyroxene porphyroclasts are assumed to belong to the kinetically controlled domain.

These conditions are mostly fulfilled in the studied Horoman plagioclase lherzolite at least after garnet became unstable, because of the presence of fine-grained aggregates. The current grain size of the fine-grained aggregate is of the order of 10–100 μm, which may have been much smaller during the main reaction stage, whereas the porphyroclastic orthopyroxene is 1–5 mm in size. This size contrast ensures quicker reactions in the fine-grained aggregate compared with diffusion in the orthopyroxene porphyroclasts. Because spinel and plagioclase are present mostly in the fine-grained aggregate, rapid grain boundary diffusion ensures that the surface Al contents of the orthopyroxene track near-equilibrium values as decompression proceeds. These conditions were not realized when garnet was stable, but diffusion within garnet crystals may not be so important in modifying the

Al content in orthopyroxene in a fertile lherzolite. Rapid reaction and transportation through grain boundaries are sufficient to justify application of the model to decompression through the garnet stability field.

In accordance with the model, we may be able to assume: (1) no grain growth or dissolution of large orthopyroxene grains; (2) local equilibrium at the grain surface; (3) perfect equilibrium in the matrix; (4) high volume fraction of fine-grained matrix as compared with pyroxene porphyroclasts. Additional assumptions made in this paper are: (5) spherical orthopyroxene porphyroclasts; (6) initially homogeneous Al concentration; (7) CFMAS system with $Mg/(Mg + Fe) = 0{\cdot}9$. The studied orthopyroxene porphyroclasts are not strongly elongated and the aspect ratio measured in thin section is $< 0{\cdot}5$.

The aforementioned model is cast into a spherical diffusion problem with a given surface Al concentration as a function of time, and is expressed by the following equation and initial and boundary conditions:

$$\frac{\partial c}{\partial t} = D\nabla^2 c \tag{1}$$

$$\left.\frac{\partial c}{\partial r}\right|_{r=0} = 0, \quad c(t, a) = f(t) \tag{2}$$

$$c(0, r) = c(0, a) = f(0) \tag{3}$$

$$D(t) = D_0 \exp\left[-\frac{E}{RT(t)}\right] \tag{4}$$

where $c(t, r)$ is the Al concentration as a function of time and distance from the core of an orthopyroxene sphere with radius a, $c(t, a) = f(t)$ is the surface concentration, and $T(t)$ is the absolute temperature at a given time. The first equation is the diffusion equation for composition-independent diffusivity, (2) is the boundary condition, and (3) is the initial condition. The diffusivity of Al is expressed by equation (4), where D_0 is the pre-exponential term, E is the activation energy, and R is the gas constant. This spherical problem can be reduced to a linear problem by introducing a new variable $u = cr$. After replacing the real time t by the compressed time τ (Lasaga, 1983), which is defined by the equation

$$\tau = \int_0^t \exp\left[-\frac{E}{R}\left(\frac{1}{T(t')} - \frac{1}{T(0)}\right)\right] \mathrm{d}t' \tag{5}$$

to make the factor in the right-hand side of equation (1) time-independent, the equations (1)–(3) become

$$\frac{\partial u}{\partial \tau} = D(0)\frac{\partial^2 u}{\partial r^2} \tag{6}$$

$$u(\tau, 0) = 0, \quad u(\tau, a) = F(\tau) = af(\tau) \tag{7}$$

$$u(0, r) = u(0, a) = rF(0) = rf(0) \tag{8}$$

respectively. Equation (6) can be non-dimensionalized by setting $u = f(0)a\,u'$, $r = a\,r'$, and $\tau = \tau_0\,\tau'$, where τ_0 is the maximum compressed time and can be obtained by integrating (5) until the value τ does not change significantly. After dropping the primes, the non-dimensionalized equations become

$$\frac{\partial u}{\partial \tau} = \kappa\frac{\partial^2 u}{\partial r^2} \tag{9}$$

$$u(\tau, 0) = 0, \quad u(\tau, 1) = \hat{f}(\tau) \tag{10}$$

$$u(0, r) = r$$

$$0 \le \tau \le 1, \quad 0 \le r \le 1, \quad \hat{f}(\tau) = \frac{f(\tau)}{f(0)} \tag{11}$$

where κ is a dimensionless parameter representing the ratio of the maximum compressed time τ_0, which corresponds to the effective cooling time scale against the diffusion time scale at the initial condition. This parameter is expressed as

$$\kappa = \frac{\tau_0}{(a^2/D(0))}. \tag{12}$$

Equation (9) has an analytical solution (Carslaw & Jaeger, 1959), but the corresponding finite element equation was solved because the boundary condition at $r = 1$ cannot be expressed in a simple integrable form.

In the model calculation, the Al concentration of orthopyroxene as a function of P–T is taken from Gasparik (1987). Grain diameter, activation energy and the pre-exponential term for Al diffusion in orthopyroxene used in the following calculation are 5 mm, 4×10^5 J/mol and $1{\cdot}94 \times 10^{-3}$ m^2/s, respectively. The diffusion data are after Smith & Barron (1991). Because of the large uncertainty in the diffusivity data, the estimated absolute decompression rate and P–T path inevitably have large errors. Ozawa (1997) examined the effect of decompression rate and P–T path on the frozen-in Al zoning profile by performing a comprehensive parameter study.